Exploring the Relationship Between Cingulate Glutamate Concentration and Resting-State Brain Dynamics: A Multimodal Imaging Study

Andrew L Frankini

Supervisor: Owen O'Daly, PhD

Centre of Neuroimaging Sciences
Institute of Psychiatry, Psychology & Neuroscience
King's College London
University of London

Thesis in partial fulfilment for the degree of MSc in Neuroscience September, 2022.

Word Count

Word Counts:	*Title*: *Abstract* (max. 350): *Main Body* (7,500-10,000; word count does not include Title, Abstract, References and Appendices; see Module Handbook):	15 350 9614

Personal Statement:

Data used in the present study was collected as a part a larger study in 2019. Dr. O'Daly and I developed the data analysis plan, along with guidance on LEiDA from Marie-Stephanie Cahart. Dr. Lythgoe supported throughout the MRS data processing.

Abstract

Introduction: The anterior cingulate cortex (ACC) plays an important role in regulation of emotion, attention, and motivation; there is notably a high concentration of glutamate (Glx) within the region. Recent neuroimaging studies have examined neural or neurotransmitter activity and their relationship to brain functional connectivity (FC). However, most explorations of FC have misleadingly modelled connectivity as unchanging within the scan session, as the brain is characterized by dynamic functional reorganisation of networks. Little is known about the relationship between cingulate Glx concentration and FC dynamics in relation to both the intercingulate (between cortical regions) and the intracingulate (within the ACC).

Objectives: Using multimodal imaging, magnetic resonance spectroscopy (MRS) and resting-state functional magnetic resonance imaging (rsfMRI), the present study aimed to determine whether individual differences in intercingulate and intracingulate brain state behaviours are associated with individual differences in [Glx] in the ACC. We aimed to determine whether a parcellation of the ACC could provide insight into dynamic intracingulate brain states.

Methods: During a single visit, rsfMRI and MRS scans were taken for thirty healthy participants who partook in a larger study. The intercingulate and intracingulate state dynamic functional connectivity (dFC) were charactised using the leading eigenvector dynamics analysis (LEiDA) approach. ACC [Glx] was processed through LCModel. Correlations were carried out to establish a relationship between ACC [Glx] and inter- and intra-cingulate brain-state characteristics.

Results: The ACC was a transiently constitutive part of two states that are broadly consistent with somato-motor network. We also demonstrated dFC changes between different regions within the ACC. When exploring the relationship between [Glx] and the dynamic behavior of these states, we found [Glx] was significantly associated with the probability of coupling between the ACC and the somato-motor state. Within the ACC, we found phase synchrony in seeds located in the MRS voxel and regions of the ACC known to be linked with ACC function. These results, however, did not survive multiple comparisons correction.

Conclusion: The ACC is an important hub for multiple networks and there are multiple subregional interactions. However, the behavior of these networks across participants does not seem to be reflective of ACC [Glx].

Table of Contents

1. Introduction

Recent neuroimaging studies have examined neural or neurotransmitter activity and brain functional connectivity (FC), the association of brain activity that occurs in distinct regions over a period of time, more closely. Specifically, there has been a growing interest in neurotransmitter signalling and its influence on both functional integration and functional specialization of the brain. Previous FC studies have taken a misleading perspective that FC is static, while contemporary research has indicated the brain is a dynamic system that changes over time. This dynamic perspective has been gaining appreciation to study FC. According to this perspective, little is known about how the FC dynamics are related to neurotransmitter concentrations, such as glutamate (Glu). Abnormal Glu concentrations have been implicated in the psychopathology of several disorders, including major depressive disorder (MDD) and schizophrenia. Evidence from pharmacological MRI studies suggest abnormal Glu signalling, specifically in the anterior cingulate cortex (ACC), might be involved in the presentation of depressive symptoms. In one particular study, patients were treated with ketamine, a non-competitive *N*-methyl-*D*-aspartate receptor antagonist which acts to normalize Glu signalling in the ACC, demonstrated ketamine's anti-depressive effect (Deakin et al., 2008). This finding strongly implicates ACC as a region of interest when considering glutamate signalling in relation to FC, where FC can be understood as the relationship of discrete neural activity across different brain regions. Indeed, a study performed by Wong et al. (2016) found a significant correlation between Glu signalling in the ACC and FC. They saw a reduction in FC of the subgenual ACC (sgACC), as well as the hippocampus, retrosplenial cortex, and thalamus in healthy males following ketamine infusion. Taken together, these studies suggest Glu signalling may modulate the FC of the cingulate cortex. However, a clear link between the Glu activity and dynamic FC (dFC) among a healthy population remains unknown.

1.1 Glutamate

L-Glutamate (Glu) is the predominant excitatory amino acid neurotransmitter in the central nervous system, estimated to be involved in the signalling processes of approximately sixty percent of neurons (Javitt, 2004). Glu plays a role in many functions of the brain, including learning and memory (Jing et al., 2000). However, abnormal Glu concentrations and overall Glu dysfunction may underly several neurodegenerative (i.e., amyotrophic lateral sclerosis and Alzheimer's disease) and psychiatric disorders (i.e., bipolar disorder, major depressive disorder, and schizophrenia) (Carriedo et al., 1996; Mattson et al., 1992; Matosin et al., 2014; McOmish et al., 2016; Cosgrove et al., 1991; Lewernez and Maher, 2015; Li et

al., 2019). Studying abnormal Glu signalling provides insight into the onset of psychiatric symptoms. In a study by Gallinat et al. (2016), Glu concentrations in the ACC were observed to be significantly lower in patients with schizophrenia as compared to healthy controls, thus resulting in the severity of schizophrenic symptoms.

There is considerable heterogeneity in Glu signalling within the general population, which may manifest in differences in brain processes. Moreover, there is evidence that individual differences in Glu in the healthy population are linked to sub-clinical symptoms of disorders (i.e., anxiety), as is seen in Modi et al. (2014). Modi et al. (2014) found that healthy participants with high anxiety scores had increased ACC Glu concentration. Furthermore, anxiety traits caused abnormal changes to brain volume in the hippocampus and amygdala in participants with no prior history of psychiatric disorders (Baur et al., 2012). Taken together, Modi et al. (2014) and Baur et al. (2012) provide evidence that, despite heterogeneity of Glu signalling in a healthy population, there is an observable variation between sub-clinical psychiatric symptoms, neurochemistry, and brain structure.

1.2 Quantifying Glu Concentrations

While there are many methods to track neurotransmitter function such as high-performance liquid chromatography, most methods are highly invasive and typically only suitable for preclinical animal work. However, proton (1H) magnetic resonance spectroscopy (MRS) is a non-invasive method and has been used to study Glu. MRS is a neuroimaging method used to analyze endogenous compounds and metabolites *in-vivo* (Ramadan et al., 2013). This neuroimaging method relies on radiofrequencies emitted by the nuclei of molecules to quantify the concentrations of compounds in the brain (Alger, 2009). MRS is similar to magnetic resonance imaging (MRI), such that both identify compounds in the brain using nuclear magnetic resonance (NMR) signals to produce anatomical depictions (Alger, 2009). These signals are produced which atomic nuclei is placed in a perpendicular and parallel magnetic field and produce a radiofrequency when perpendicular magnetic field is turned off (Chatham and Blackband, 2001). While MRI detects NMR signals from water protons in the brain tissue, MRS detects NMR signals from protons of biochemical compounds, such as Glu and Gln (Alger, 2009). The NMR signals that are detected are communicated as a frequency spectrum, and the peaks formed on the spectra can be used to calculate the concentrations of the metabolites (Tognarelli et al., 2015).

While absolute Glu concentrations can be determined at high scanner field strength with MRS using LCModel data fitting software package, Gln is typically analyzed together with Glu – the combination

thereof is denoted as Glx (Govindaraju et al., 2000). Glx concentrations are understood as the summation of Glu and Gln concentrations ([Glx] = [Glu] + [Gln]). A definitive distinction between the two compounds through MRS is difficult to achieve at the lower field strengths, typically available due to the structural similarities between Glu and Gln; which is reflected in similar NMR spectra (Govindaraju et al., 2000; Ramadan et al., 2013).

An important question to ask is the degree to which such variation in glutamate or Glx concentration is functionally relevant. The degree of variation in Glx in regional FC is one area of growing interest due to evidence that Glx is related to cognitive performance, as seen in lower Glx concentrations in patients who suffer from schizophrenia (Falkenberg et al., 2014). Consistent with this perspective, Siegel-Ramsay et al. (2021) studied Glx concentrations of the dorsal ACC and the effect on FC, by comparing patients with autism spectrum disorder (ASD) to healthy controls. The healthy controls were seen to have a positive correlation of [Glx] to FC between the dorsal ACC and limbic, parietal, and insular regions; while patients with ASD showed a negative relationship between the [Glx] and the same regions (Siegel-Ramsay et al., 2021). Despite these particularly interesting findings, one limitation of the study was the dependence on the idea of static functional connectivity. Increasingly, there is a growing appreciation of the degree to which the brain is a dynamical system, and the consideration that associations underlying FC are often transient. Furthermore, the use of Pearson's correlation with static functional connectivity is likely suboptimal since static FC averages the scan's timeseries. Thus, dynamic functional connectivity (dFC) and its relationship with [Glu] in the ACC ought to be studied further.

1.3 Dynamic Functional Connectivity

FC refers to the temporal association of neural activity across distinct brain regions (Eickhoff and Muller, 2015; Friston 1994). It can be thought of as an association of brain activity across different regions of the brain. FC differs from structural connectivity, in that structural connectivity refers to a physical interconnectedness between brain structures, while FC is a statistical measurement of the correlation of activity between different brain regions (Uddin, 2013). By studying FC, researchers can draw potential inferences concerning functional interactions between distinct brain regions (Gaudet et al., 2020). That means, brain regions can be functionally connected but have no direct structural connections (Honey et al., 2009).

Traditionally, the FC of brain regions is studied through resting-state functional magnetic resonance imaging (rsfMRI) by revealing the statistical interdependence of neural activity across distinct brain regions

using *Blood-Oxygen-Level-Dependent* (BOLD) signals (Hancock et al., 2022; Friston 1994; Hillman, 2014). The BOLD signals reflect reactive hyperaemia and the delivery of oxygenated blood, which point to increased brain activity because blood flow indicates increased cellular activity (Hutchinson et al., 2013). This approach relies on the notion that such functional associations are stationary (unchanging) across time, and commonly involves framing FC in terms of the Pearson correlation coefficient (Menson and Kirshnamurthy, 2019).

Recently, however, neuroscientists interested in studying FC have found the brain is a dynamical system; thus, forming coalitions of brain regions to accommodate for changing and coordinated networks of activity underlying neural processes. This interest has increased the proportion of studies that examine dynamic functional connectivity (dFC) changes, as quantified by Pearson's correlation on continuous window data segments (Menson and Kirshnamurthy, 2019). The dFC assumes that the FC of the functional network in the brain is ever changing, such that there is a perpetual and simultaneous change in activity across the functional network (Adeo-Jury et al., 2020, Guo et al., 2004). In turn, these changes in activity across brain regions reflect different brain states, which are defined as *quasi*stable condition-dependent arrangements of networks, usually dynamically coupled, during a period of activity (Deco et al., 2019). Brain states are thought to have three essential characteristics: (i) rate of occupancy, or the percentage of total time in a certain brain state; (ii) lifetime, or the average duration of a brain state; (iii) transition, or the probability that a certain brain state switches to another (Taghia et al., 2018; Martinez et al, 2020). Furthermore, brain states seem to be affected by illnesses and disorders (Sendi et al., 2021). A study performed by Sendi et al. (2021) investigated dFC and major depressive disorder and found symptom severity was linked to disrupted dFC and increased transitioning of some brain states in the ACC (i.e., states with low ACC FC to a state with high ACC FC). Thus, of interest for the present study would be which brain states of the ACC are involved in intracingulate activity within the ACC and intercingulate activity related to other brain regions.

1.4 Anterior Cingulate Cortex

The ACC is one of four functionally distinct regions of the cingulate cortex, the others being: retrosplenial cortex, posterior cingulate cortex (PCC), midcingulate cortex (Vogt et al., 1995). It is in Brodmann areas (BAs) 24, 25, 32, and 33 and can be broken down into three subregions based on cytoarchitecture, or cellular composition, and functionality (Vogt et al., 1995; Margulies et al, 2007). The subregions of the ACC consist of the dorsal ACC (dACC), the pregenual ACC (pgACC), and the sgACC (Alexander et al., 2021). The latter two subregions (pgACC and sgACC) also make up the part of the rostral

ACC (rACC) (Lee et al., 2018; Palomero-Gallagher et al., 2008). Depending upon point of reference made in the brain, the dACC can also be known as the caudal ACC (Stevens et al., 2011). The ACC is a structure located directly above the corpus callosum, which seems to be involved in information processing, specifically relating to emotion, memory, and decision making (Jumah and Dossani, 2021). Additionally, the ACC seems to be involved in the motor command pre-processing, which occurs before the action of the motor command is directed from the primary and supplementary motor cortex to the spinal cord (Jumah and Dossani, 2021).

The ACC acts as a central node in the salience network, along with the anterior insula. The salience network is implicated in the regulation of anti-correlated associations between the default mode network (DMN) and fronto-parietal network (FrPar) (Goulden et al., 2014). The salience network achieves this regulation by mediating the switching of brain states in response to changes in the external or internal environment (Goulden et al., 2014). While the ACC and insular cortex are structurally connected, evidence suggests the ACC is also functionally connected to other intercingulate regions (Van den Heuvel et al., 2009). In a study by Margulies et al. (2007), the inferior rACC demonstrated consistent patterns of activity with the limbic and paralimbic regions, including in the ventromedial prefrontal cortex, hippocampus, posterior cingulate cortex, and amygdala (Margulies et al., 2007). It was also established that the caudal ACC displayed consistent activity with the frontoparietal regions involved in sensorimotor processes (Margulies et al., 2007).

Functional intracingulate connectivity has yet to be investigated in humans. Studies have investigated the intracingulate structural connectivity, but only in non-human animals, such as rats and macaque monkeys (Jones et al., 2005; Parvizi et al., 2006). Jones et al. (2005) found the ACC in rats displayed high structural intracingulate connections, demonstrated by the caudal part of the dACC projecting to the caudal area of the ventral ACC, while the whole ventral ACC projects to the mid-rostro-caudal dACC. Furthermore, the caudal supracallosal ACC, a structure within the dACC, is connected to the rostral retrosplenial cortex in both the forward and reverse direction, and the rostral supracallosal ACC is interconnected with the caudal retrosplenial cortex (Jones et al., 2005). Further evidence for the intracingulate connectivity of the ACC is provided by Parvizi et al. (2006), who observed neural connections of the posteromedial cortex in macaque monkeys. The posteromedial cortex consists of areas in the posterior cingulate, retrosplenials, and mesial parietal (Parvizi et al., 2006). They found that the ACC projects (BA 24a and 24b) connections to the posterior cingulate BA 23a and 23b and the retrosplenial BA 29 and 30 (Parvizi et al., 2006). While these studies support the notion that the ACC is structurally connected in non-humans to other cingulate subregions, dFC in humans has yet to be demonstrated.

1.5 Current Novel Study

While previous research has studied the dFC of the ACC, limited research has been conducted on Glu in relation to different brain states. In the present study, the relationship between [Glx] in the ACC and the dynamic coupling of discrete regions of this structure will be investigated. Specifically, we will investigate whether varying levels of [Glx] affect the characteristics of discreet brain states. We will aim to characterise the dFC of the ACC, both with respect to intrinsic intracingulate brain states, as well as with intracingulate brain states of regions commonly known to interact with the ACC. This study will use a multi-modal approach, using both rsfMRI and MRS scanning data from a cohort of healthy subjects. We hope to determine if any of the core characteristics of identified brain states are associated with individual differences [Glx] in the ACC concentration. We hypothesize that there will be several brain states identified in both the intercingulate and intracingulate regions that shown synchrony with the ACC. Furthermore, we hypothesize that the [Glx] in the ACC will demonstrate a significant correlation with brain state characteristics, as characterized by LEiDA.

2. Methods

2.1 Participants and Procedure

Thirty healthy adults (Male = 14, Female= 14, Unknown = 2), aged 22 to 59, were recruited and participated in the study between May 2019 and September 2019. All participants had no known history of neurological or psychiatric disorders and were not taking any psychotropic medications. Demographics played no role in selection criteria, and each participant was asked to abstain from caffeine on the morning of the fMRI scan. Each participant provided written informed consent (ethics number HR-18/19-11058; King's College London Psychiatry, Nursing & Midwifery Research Ethics Subcommittee) and attended a single scanning session at the Centre for Neuroimaging Sciences -- part of the Institute of Psychiatry, Psychology and Neuroscience, King's College London.

2.2 Study Design

The present study used data that was a part of a larger multi-modal imaging study, which consisted of a single visit multimodal fMRI scan that took place over 90 minutes. Prior to the scan, participants were asked to answer questionaries (Big Five Personality Traits, Warwick-Edinburgh Mental Wellbeing Scale, and Multidimensional Mood State Questionnaire), and received task-related training for task-related scans. The data was acquired from resting state multi-band fMRI and MRS scans, and explored the relationship between ACC [Glx] and resting-state dynamics in both intercingulate and intracingulate regions of healthy participants. The three objectives of this study are as follows: (1) analysis of rsfMRI dFC using the *Leading Eigenvector Dynamics Analysis* (LEiDA) framework in both intercingulate and intracingulate regions; (2) analysis of MRS corrected ACC Glx concentration scaled to unsuppressed water; (3) correlation of corrected scaled Glx concentration to occupancy, lifetime, and transition of brain states calculated using LEiDA through simple linear regressions.

2.3 Data Collection

For the MRI data acquisition, all participants were scanned in a 3 T MR scanner (Discovery MR750, General Electric, Milwaukee, WI, USA). During each scanning session, each participant underwent both a multi-band rsfMRI and a T1-weighted anatomical MRI. The multi-band rsfMRI was chosen over the more common multi-echo rsfMRI because the multi-band rsfMRI typically has a shorter repetition time (T_R) (around 0.7 – 1 sec) (Tong et al., 2014). The multi-band rsfMRI acquisition protocol

was as follows: echo time (T_E) = 30 ms; repetition time (T_R) =750 ms; flip angle = 63°; slice thickness = 3.3 mm; field of view = 211 mm^2; matrix size = 64x64 mm; multi-band factor = 4; ARC = 1; number of time points = 652. The MPRAGE (Magnetization-prepared rapid gradient-echo) T1-weighted anatomical MRI had the following parameters: T_E= 3.02 ms; T_R= 7.3 ms; inversion time = 400 ms; flip angle = 11°; slice thickness = 1.2 mm; field of view = 270 mm^2; matrix size = 256x256 mm; spatial resolution = 1 mm^3.

In addition to the whole-brain imaging, data for the [Glx] in the ACC was collected using a PRESS (point-resolved spectroscopy) H^1 MRS sequence. The PRESS H^1 MRS was set up according to the following protocol: T_E = 30 ms; T_R =3000 ms; flip angle = 90°; slice thickness = 20 mm; field of view = 240 mm^2; matrix size = 1x1 mm; spatial locations: 1. For this scan, one 20 x 20 x 20 mm voxel with the centre placed 16 mm above the corpus callosum genu and perpendicular to the ACC'S bicommissural line was measure, which consisted of the ACC. Following collection of scans, both the MRI data and MRS data were separately pre-processed.

2.4 rsfMRI Data

2.4.1 Pre-processing

For the MRI data pre-processing, the Statistical Parametric Mapping (SPM12; Wellcome Trust Centre for Neuroimaging, UCL, London, UK) software package from MATLAB R2020a (MathWorks, Natick, MA, USA) was used in addition to a toolbox of CONN Version 18b (Whitfield-Gabrieli and Nieto-Castanon, 2012). The CONN toolbox was used to pre-process the multi-band rsfMRI images. As rsfMRI data is vulnerable to noise created by motion, pre-processing the data allows for correction of the noise and thus allowing the data to be studied between different cohorts. The pre-processing pipeline used in the present study for resting state functional data is shown in **Table 1**.

Order	Pre-processing
1	Realignment and unwarping
2	Scrubbing of outliers
3	Image Coregistration
4	Unified Segmentation
5	Indirect Normalisation to Montreal Neurological Institute (MNI) standardized space

Table 1: Order of Pre-processing steps

First, realignment and unwarping were utilised to correct for artefacts, which occurred due to participants' motion in the scanner. However, other, more subtle motion-related artefacts could still be present. Therefore, outlier signals caused by other artefacts were corrected for using the artefact rejection tool (ART). Following this, image coregistration was used to confirm the alignment of rsfMRI functional images with structural image produced by the anatomical MRI. Next, unified image segmentation classified the tissue type of each voxel (i.e., grey matter voxel, white matter voxel, etc.) of the T1-image. Lastly, indirect normalisation of the functional data took place by warping the images to the standard space, known as the Montreal Neurological Institute (MNI) space using warp parameters estimated from the structural scan. Indirect normalisation was used because structural imaging has better grey-white contrast, higher resolution, and better signal-to-noise ratio.

In addition to rsfMRI data pre-processing pipeline, the CONN toolbox (Whitfield-Gabrieli et al., 2012) was used to denoise the pre-processed images by removing any remaining artefacts which have not been extracted. Denoising images increases the single-to-noise ratio of the scan allowing for greater spatial resolution of the signal. To create the denoised image, a bandpass filter of [0.008,0.09] Hz, linear detrending, and despiking after regression was performed on the pre-processed rsfMRI images for all participants. Of note, smoothing of images during pre-processing did not occur for this present study. Smoothing can lead to a loss of spatial specificity, the loss of a MR signal in space, and as this study focuses on observing the dFC in the ACC, which is dependent on spatial specificity and the spatial resolution of the signal. Furthermore, since the analysis of the data focused on extracting the timeseries, smoothing the data may result in removal of important signals that are pertinent to dFC

2.4.2 ROI Creation

2.4.2.1 Intercingulate ROIs

Following the pre-processing, region of interest (ROI) for both intercingulate and intracingulate seeds were needed to be defined. 32 ROIs associated with common resting-state networks (i.e., default mode network, sensorimotor network, visual network, salience network, dorsal-attention network, fronto-parietal network, language network and cerebellar network) were defined by Conn's ICA analyses of HCP dataset (Whitfield-Gabrieli et al., 2012). **Appendix 1** contains the coordinates and names of the intercingulate ROIs. The ROIs were then extracted and applied to the pre-processed functional images using MarsBaR (Bret et al., 2002) to extract the mean timeseries of the voxels in each ROI.

2.4.2.2 Intracingulate Seeds

A study observing the functional connectivity of the ACC in multi-echo rsfMRI, Margulies et al. (2007) generated 32 spherical ROI seeds in the ACC (1 x 1 x 1 mm, radius = 3.5 mm) by fitting a quadratic function along the corpus callosum curve as a reference. Two types of seeds were identified and created in each hemisphere, 9 inferior and 7 superior seeds (16 seeds in each hemisphere, 32 seeds in total) (Margulies et al., 2007). The inferior seeds were located 5 mm above the curve with the superior seeds approximately 15 mm above the curve, each separated by 10 mm (Margulies et al., 2007). The present study uses these ROI seeds in the ACC as generated by Margulies et al. (2007). **Table 2** contains the MNI coordinates for each of the 32 seeds with Figure 1 displaying the 16 seeds of one hemisphere on the MNI brain. The ROIs were defined using MarsBaR (Bret et al., 2002), a toolbox of SPM. The newly defined ROIs were then applied to the pre-processed functional images to extract the mean timeseries of the voxels in each ROI. The type of analysis performed for intracingulate seeds was a seed-to-seed correlation analysis, which correlates specified seeds with seeds containing activity.

Seed Name	X coordinate	Y coordinate	Z coordinate	Seed Name	X coordinate	Y coordinate	Z coordinate
i1+	5	-10	37	s1+	5	-10	47
i1-	-5	-10	37	s1-	-5	-10	47
i2+	5	0	36	s2+	5	2	46
i2-	-5	0	36	s2-	-5	2	46
i3+	5	10	33	s3+	5	14	42
i3-	-5	10	33	s3-	-5	14	42
i4+	5	19	28	s4+	5	25	36
i4-	-5	19	28	s4-	-5	25	36
i5+	5	27	21	s5+	5	34	28
i5-	-5	27	21	s5-	-5	34	28
i6+	5	34	14	s6+	5	41	21
i6-	-5	34	14	s6-	-5	41	21
i7+	5	38	6	s7+	5	47	11
i7-	-5	38	6	s7-	-5	47	11
i8+	5	34	-4				
i8-	-5	34	-4				
i9+	5	25	-10				
i9-	-5	25	-10				

Table 2: Coordinates of ACC seeds generated by Margulies et al., (2007); i = inferior seeds s = superior seeds; + = right hemisphere, - = left hemisphere.

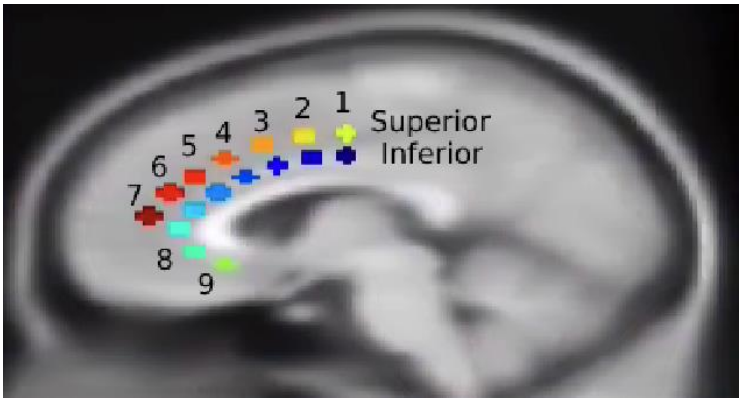

Figure 1: 16 seeds spatial location on ACC; image captured using MarsBaR

2.5 dFC Analysis using LEiDA

The dFC of the ACC was explored using LEiDA (adapted from Cabral et al. (2017)), a suite of scripts written for MATLAB R2020a (MathWorks, Natick, MA, USA). The purpose of this framework is to characterise the phase-locked oscillatory patterns in connected dynamic networks, classified as "brain states" (Cabral, 2021). In the present study, LEiDA was used to investigate the resting-state dFC within the ACC (intracingulate), and dFC between the ACC (intercingulate) and overlapping known functional

networks that were defined by Yeo et al. (2010). The known functional Yeo networks used to overlap were dorsal attention network (DorAtt); fronto-parietal network (FrPar); limbic network (Limbic); ventral attention network (VenAtt); dorsal attention network (DorAtt); somato-motor network (SMot); visual network (Vis).

LEiDA detects synchronous patterns of neural activity between distinct brain regions and across functional networks. This framework relies on BOLD signals as a time-series produced by rsfMRI (Cabral, 2021). These signals are manipulated using the Hilbert transform (HT) into complex analytic signal associated with a phase. Since BOLD signals are time-varying, the Hilbert transformed data expresses its analytic signal as a product of both the time-varying amplitude and the cosine of the time-varying phase angle (Cabral, 2021). In more detail, HT quantifies both the imaginary (denoted as the sine of the phase angle) and real parts of the signal (denoted as the cosine of the phase angle). Through the summation of these two components (real and imaginary), the analytic signal is produced (Cabral, 2021).

The transformed signal was used to identify the phase orientation of the 32 ROI seeds at timepoint t (t_{total} = 644 seconds) to further calculate the degree of phase synchrony, represented as a matrix of dynamic phase coherence (dPC). The dPC determines how well the phases are in-phase (synchronous) or out of phase (anti-phase) over time. More specifically, patterns of phase synchrony were acquired by the evaluation of phase coherence between ROI x and ROI y at each t, dPC(x,y,t), using equation (1). This equation produces the dPC matrix on a range of -1 (total anti-phase between x and y) to 1 (total phase synchrony between x and y) (Farinha et al., 2022).

$$dPC(x,y,t) = cos\ (\ (x,t) -\ \ (y,t)) \qquad \textbf{(1)}$$

In this study, the dPC was calculated at every time point for every combination of the 32 seed ROIs for each participant. Following this, the leading eigenvectors $V_1(t)$ (dimension Nx1, N= number of ROIs), signifying the dominant connectivity pattern of each dPC(t) in every seed, was computed to determine the phase coherence patterns (Cabral et al., 2017). Phase coherence or orientation had either positive or negative projections which indicated what ROIs were in synchrony with each other and which ones were not in synchrony. Thus, direction of projections was determined using $V_1(t)$. The directions of the projections were significant as multiple phases projecting in the same orientation were identified as being part of a given, synchronised network of ROIs (also called cluster or state) that dominate at a specific timepoint.

Once synchronised networks of ROIs were identified, K-mean clustering was employed on all $V_1(t)$ to determine the optimal number of clusters/states by grouping data based on similarities. The K-means algorithm initially assigned each $V_1(t)$ to a specified number of clusters k and calculated the centroid of the

cluster. The purpose of this algorithm was to minimise the data variation within the cluster through the reduction of the distance between the data and the centroid. In this dissertation, the K-means algorithm partitioned and clustered all $V_1(t)$ into $k_{\underline{min}} = 2$ to $k_{max} = 8$ for possible intercingulate clusters/states, and $k_{\underline{min}} = 2$ to $k_{max}=15$ for possible intracingulate clusters/states. As this study is novel reagarding the parcellation of the intraACC, the minimum and maximum number of possible states were chosen to allow for the exploration of the number of possible ACC brain states at rest. Finally, to ensure the validity of the clustering, the algorithm performed 1000 iterations, and the Dunn score, a metric used to determine the optimal number of clusters/states, was calculated to inform the final decision regarding the likely true number of states in the data.

With the number of brain states calculated, the three characteristics (occupancy, lifetime, and transition) of each brain state were measured. Occupancy referred to the percentage of total time in a certain brain state, lifetime was the average duration of a brain state on each occurrence, and transition matrix described the probability of a particular brain state shifting to another specific state (Martinez et al, 2020). The brain states along with the three characteristics were then correlated and analysed in conjunction with Glx concentrations.

2.6 MRS Pre-processing and Analysis

The PRESS MRS data of all participants was first pre-processed using SPM12 unified segmentation. Following the T1 unified segmentation, the proportion of each tissue class (grey matter (GM), white matter (WM), and cerebrospinal fluid (CSF)) within the ACC MRS voxel was calculated from the native space images produced during unified segmentation. Following SPM12, the LCModel Version 6 (Provencher, 1993) package on MATLAB 2020a was used to analyse the MRS spectra. The LCModel is a method that allows for the automatic analysis and quantification of an *in vivo* metabolite spectrum by representing the spectrum as a Linear Combination of Model *in vitro* spectra (Provencher, 2001). The LCModel measured the complete spectrum chemical shift in parts per million (ppm) produced by the PRESS H^1 MRS scan. The result of LCModel was the production of a concentration table containing absolute Glu and Gln concentration, along with other metabolites, and the concentration scaled to an internal reference, creatine, concentration in millimoles (mmol). The chemical shift of Glu ranges between 2.34 and 3.47 ppm, while Gln resonance is around 2.34 ppm (Maddock et al., 2018). Some of the other metabolites measured by the LCModel include alanine, aspartic acid, creatine, GABA, glucose, phosphocreatine, lactate, and *N*-acetylaspartate. The metabolites that were reported in this dissertation were Glu and Gln. In addition, since metabolism and many underlying pathologies may affect Glu concentration,

absolute Glu was not sufficient to use due to its effect on the global ACC Glu level. To solve this issue, the total absolute concentrations of Glu and Gln were summated to produce the absolute concentration of Glx, giving a greater confidence in the global ACC Glu concentration. Gln is a metabolite of Glu and plays a vital role in Glu recycling.

Instead of using Glx concentration scaled to the internal reference of creatine, the concentration was scaled to unsuppressed brain tissue water from the same volume. As there is no optimal internal reference (Mikkelsen et al., 2019), creatine has been often used as the reference; however, creatine has the possibility of producing a lower signal quality, and is present in both GM and WM, but not CSF (Mikkelsen et al., 2019). In the present study, Glx concentrations were scaled to internal water due to its abundance in the brain.

Glx was scaled by using an equation (2) from Near et al. (2021):

$$[M]_{Molar} = \frac{S_{M_{obs}}(f_{GM}d_{GM}R_{H2O_{GM}}+f_{WM}d_{WM}R_{H2O_{WM}}+f_{CSF}d_{CSF}R_{H2O_{CSF}})}{S_{H2O_{obs}}(1-f_{CSF})R_M}\frac{2}{N_M}[H_2O]_{molar} \qquad \textbf{(2)}$$

where $S_{M_{obs}}$ = observed metabolite signal intensity in presence of relaxation, f = voxel fraction of a given tissue class**,** d = density of water**,** R_{H2O} = relaxation time of water, N_M = number of protons contributing to signal, $S_{H2O_{obs}}$ = observed water signal intensity in presence of relaxation**,** R_M = relaxation time of Glx. The equation was modified slightly since the MRS scan was programmed to calculate the $\frac{S_{M_{observed}}}{S_{H2O_{observed}}}$ and $\frac{2(H2O_{Molal})}{N_M}$. The values for the density of water for the three tissues (GM=0.78, WM=0.65, and CSF 0.97) was taken from Near et al. (2021).

Prior to this equation (2), the correction of relaxation time occurred. The relaxation times of water and Glx for GM, WM, CSF were calculated using equation (3) from Near et al. (2021):

$$R = exp\,(-\frac{T_E}{T_2})(1 - exp\left(-\frac{T_R}{T_1}\right) \qquad \textbf{(3)}$$

where relaxation times T_1 and T_2 values of water (Table 3a) were taken from Gasparovic et al., 2006 and values for Glx (Table 3b) were taken from Srinivasan et al. (2006). This dissertation assumed that there the CSF contained no Glx as suggested in Srinivasan et al. (2006). Following the calculation using equation (2), Glx was scaled to the internal reference of water and was used in statistical analysis.

3A.

(sec)	GM	WM	CSF
T_1	1.304	0.66	2.93
T_2	0.093	0.073	0.23

3B.

(sec)	GM	WM
T_1	1.25	0.96
T_2	0.2	0.2

Table3: (A) Relaxation times T_1 and T_2 values for water in GM, WM, and CSF obtained from Gasparovic et al. (2006); **(B)** Relaxation times T_1 and T_2 values for Glx in GM and WM obtained from Srinivasan et al. (2006).

2.7 Statistical Analysis

Statistical analysis was performed on Jamovi version 2.3 (Jamovi Project, 2022), a statistical software on built on the R software version 4.1 platform (R Core Team, 2021). Three linear regressions were performed to analyse the relationship of ACC Glx concentration and the three characteristics of brain states (occupancy, lifetime, and transition) for each of the brain states that contain ACC phase synchrony, both for intracingulate and intercingulate states. For intracingulate states to be included in these linear regressions, at least two of the three seeds on the same hemisphere (s6, i6, and s7) were needed to have phase synchrony. A two-tailed t-tests with a significance p-value of 0.05 was performed for each correlation made prior to the Bonferroni correction for multiple-comparisons (p=0.001667).

Two more groups of relationships were observed: (1) exploring the relationship of state transition between intercingulate states that were dominated by default mode network and fronto-parietal network and [Glx]; (2) exploring the intracingulate relationship of probability of occurrence and mean lifetime for all other intracingulate states that do not meet the criteria of ACC seeds located within the MRS voxel and [Glx]. Correlation matrixes were run to establish if any state from both groups were significantly affected by [Glx].

3. Results

This present study assessed the relationship between [Glx] and network-based dFC, as well as with intra-ACC dFC. There was a particular interest in ROIs with transient incorporation with the ACC. Moreover, the present study explores whether individual differences in a number of ACC-related network characteristics are related to ACC [Glx].

3.1 Glutamate Concentration

To calculate the corrected [Glx] per tissue water volume in the ACC using the tissue correction formula, we measured the absolute [Glu] and [Gln] and found the absolute [Glx] through their summation. Descriptive statistics (n=30) characterizing the measured absolute [Glx], [Glu], [Gln] in the ACC, and [Glx] per tissue water volume are summarized in **Table 4.** We expected inter-individual differences in the absolute [Glu] and absolute [Gln] in the participant's ACC, leading to variations in the [Glx] per tissue water. The mean and median [Glx] per tissue water were similar (9.56 mmol/L, 9.42 mmol/L). Of the thirty participants, there was only one outlier in [Glx] (11.994 mmol/L). **Appendix 2** contains the raw data of the concentrations and the LCModel reported findings, such as the voxel fractional tissue of GM, WM, and CSF for all the participants. Any correlations between the [Glx] per tissue water volume in the ACC and brain state characteristics were reported in section 3.4.

Concentration Group	Mean	Median	SD	Minimum	Maximum
Absolute [Glx] (mmol)	10.97	10.92	1.221	8.203	13.96
Absolute [Glu] (mmol)	8.73	8.84	0.866	6.998	10.28
Absolute [Gln] (mmol)	2.25	2.13	0.762	0.830	4.35
[Glx] per tissue water (mmol/L)	9.178	9.045	1.091	7.612	11.994

Table 4: Descriptive statistics for concentrations obtained from the MRS scan

3.2 Intercingulate Brain States

LEiDA was used to examine and identify discrete and transient patterns of FC between brain regions (brain states) in which the ACC ROI were implicated. A K-means clustering algorithm was applied to all the leading eigenvectors for all participants. The output of this algorithm (k=7) revealed that the optimal number of clusters present in the intercingulate data was seven, meaning that were seven transient discrete patterns of FC seen amongst subsets of the 32 seed regions in the resting-state data (seven brain states). Two brain states (4 and 7) were determined to incorporate the ACC, and when compared to the Yeo network, the spatial extent of both these states was most consistent with Yeo's somato-motor network (SMoT), **FIGURE 2.** In other words, the activity of the ACC was in phase synchrony with states 4 and 7. Additionally, two states that the ACC regulates were state transitions between State 1 to State 2 and State 2 to State 1, most consistent with the fronto-parietal network (FrPar) and the default mode network (DMN) respectively, even though phase synchrony was not seen.

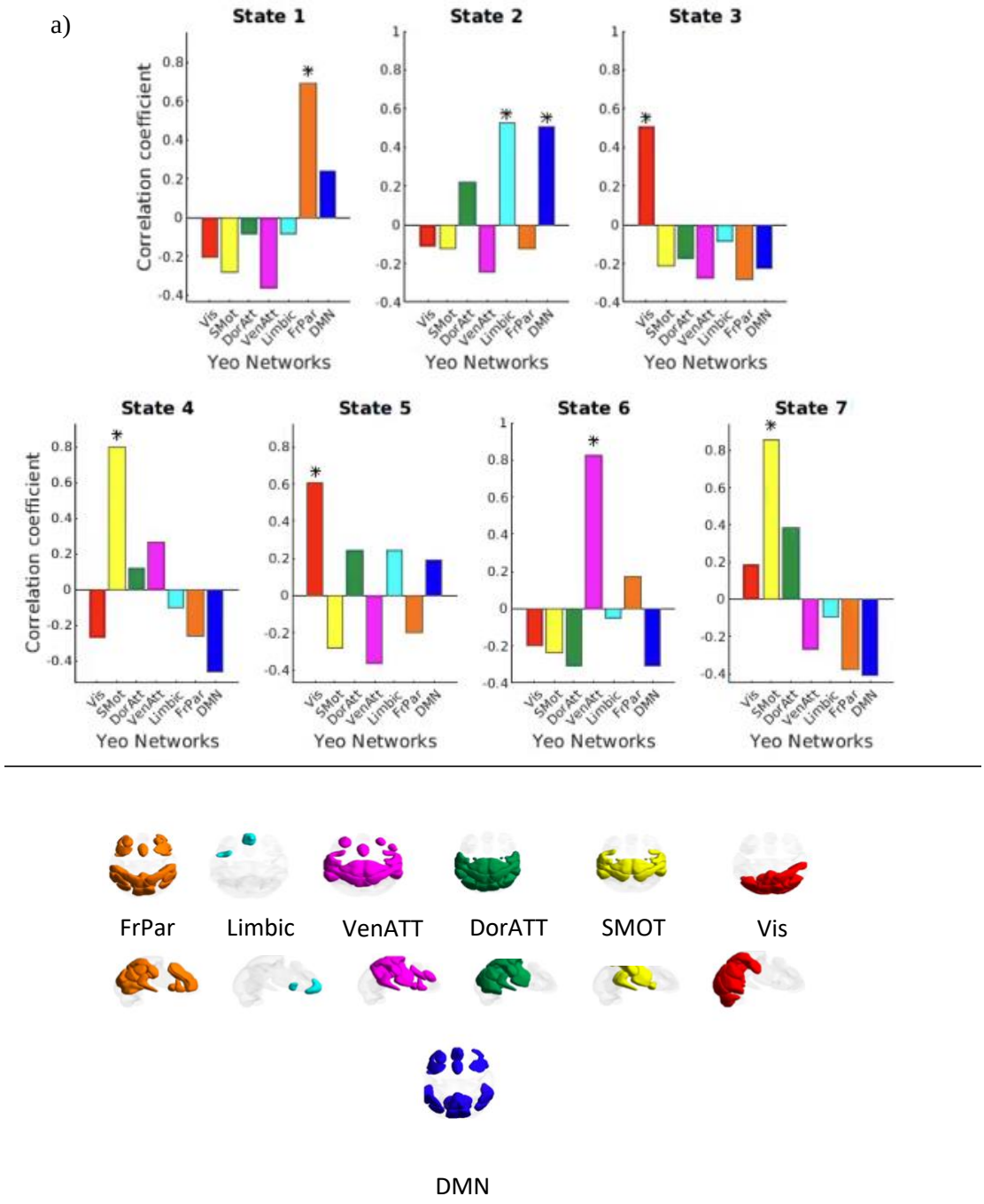

Figure 2: (a) Bar graphs of the Pearson's correlation coefficient of each brain state pattern and the seven function networks defined in Yeo et al. (2010). * Indicates significance ($p < 0.05$) of active networks of each brain state. **(b)** Representation of network ROI activation color-coordinated with overlapping Yeo network; The abbreviations of the networks are: DorAtt = dorsal attention network; FrPar = frontoparietal network; Limbic = limbic network; VenAtt = ventral attention network; DorAtt = dorsal attention network; SMot = somato-motor network; Vis = visual network.

Calculations for the probability of occurrence (Pall), mean lifetime (LTall), and probability of state transitions (ST) were done for all seven FC-based brain states. A plot for the mean Pall, mean LTall, and a probability matrix for the ST were plotted in **Figure 3** for all seven states.

a)

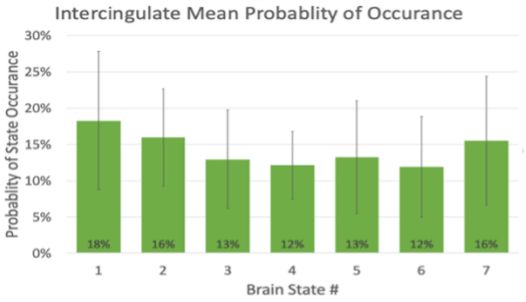

b)

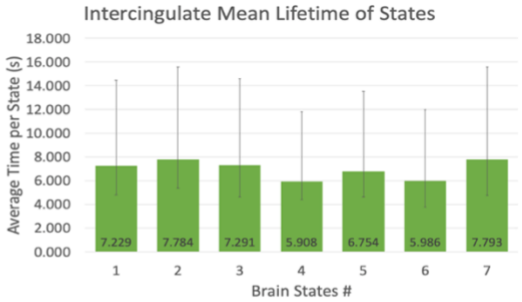

c)

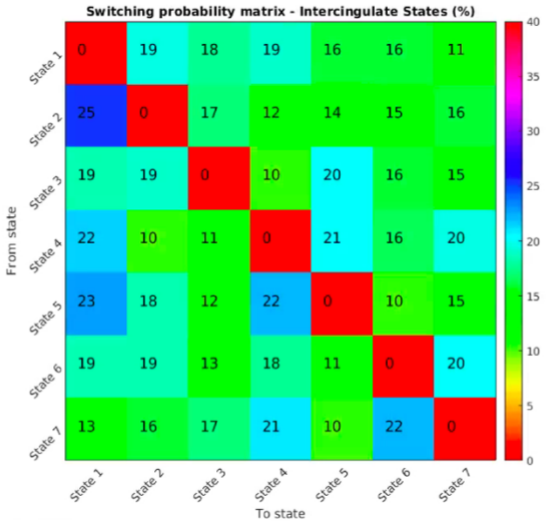

Figure 3: (a) Mean probability of occurrence in intercingulate brain states with standard deviation error bars. Graded on a percentage scale; **(b)** Mean lifetime of each intercingulate brain state standard deviation error bars. Graded in seconds; **(c)** Intercingulate state transitions probability matrix graded on a percent scale. Note: darker the hue of blue indicates higher switching probability. * indicates significance ($p < 0.05$)

3.3 Intracingulate Brain States

Next, the analysis of K-means revealed nine discrete states reflecting the interaction between subsets of our 32 ACC seed regions Unlike for the intercingulate analysis, there is no established atlas of differentiated resting state activity in the ACC. Individual ROIs constituting each state were identified and are visually represented in **Figure 4.** A complete table highlighting the active ACC seeds in States 1 through

8 is shown in **Appendix 3**; however, State 9 reflected a state with an absence of reliable phase synchrony amongst any of the ROIs.

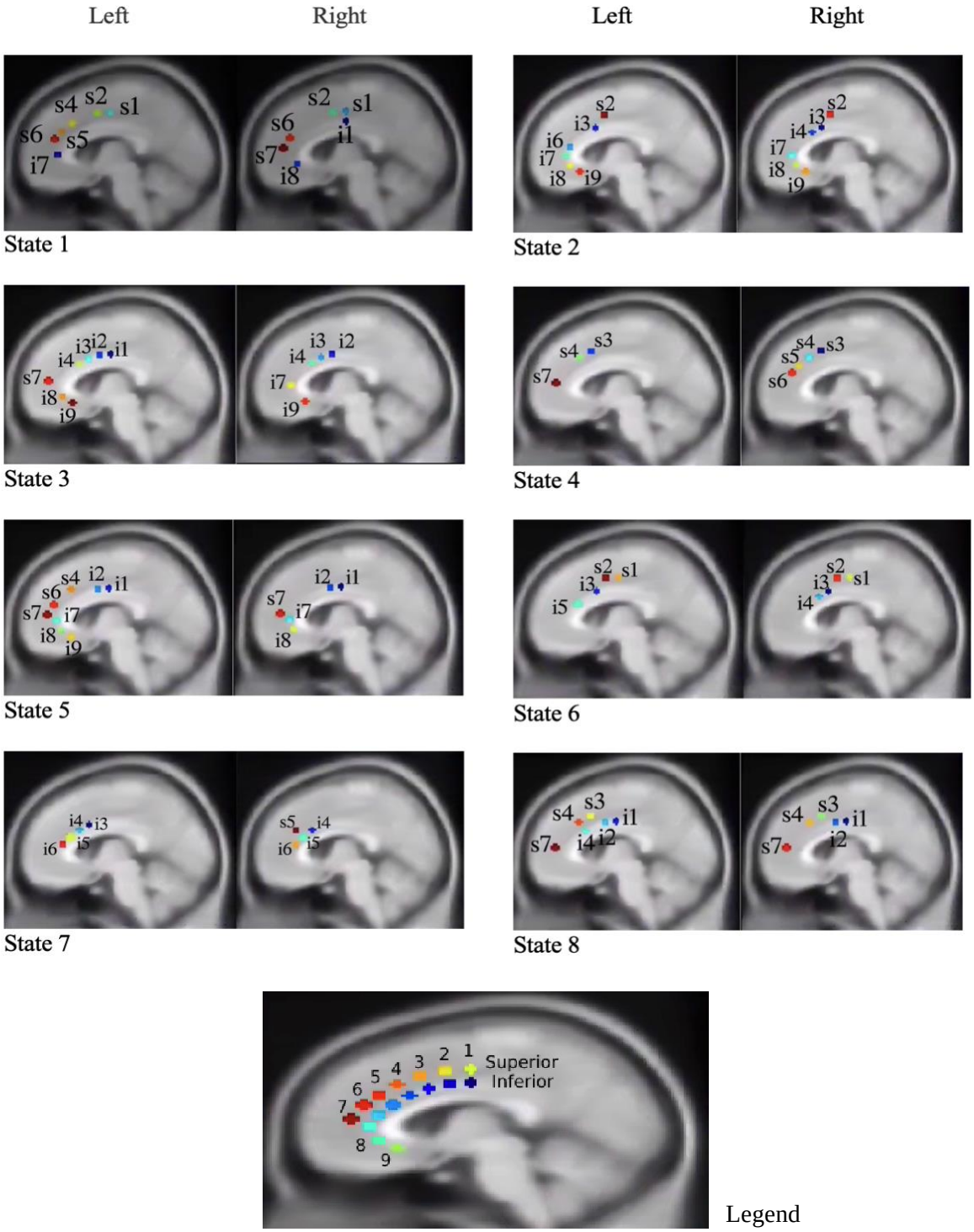

Figure 4: Active intracingulate ACC seeds present in each of the brain states; Represented in the legend is the location of every ACC seed used. Note: the seeds in legend are located on both hemispheres of the brain.

The brain state mean characteristics (probability of state occurrence, lifetime, and probability of state transition) of intracingulate states are plotted in **Figure 5.**

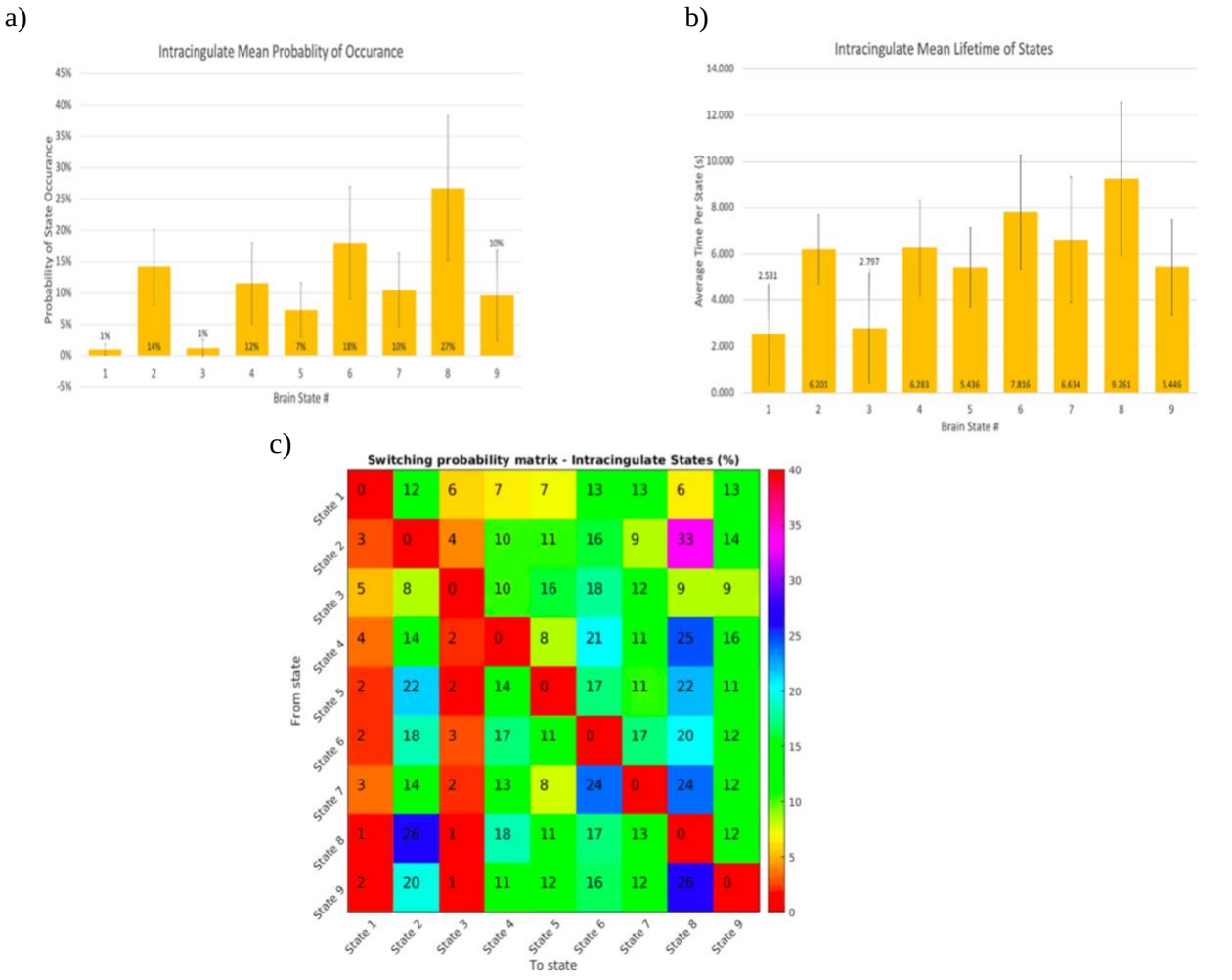

Figure 5: (a) Mean probability of occurrence in intracingulate brain states with standard deviation error bars. Graded on a percentage scale; **(b)** Mean lifetime of each intracingulate brain state standard deviation error bars. Graded in seconds; **(c)** Intracingulate state transitions probability matrix graded on a percent scale. Note: Darker the hue of blue indicates higher switching probability. * Indicates significance ($p < 0.05$).

3.4 Glx concentraion and Brain State Correlation

3.4.1 Intercingulate

The relationship between the characteristics of intercingulate brain states and the corrected [Glx] in the ACC was investiagted. It was predicted that the [Glu] in the ACC would influence intercingulate

brain states. Furthermore, it was expected the [Glu] in the ACC to play a role in transitions between brain states across the frontoparietal network (FrPar) and default mode network (DMN).

The three brain state characteristics, Pall, TaLL and ST, observed for the states that were broadly consistent with the somatomotor network, were investigated in relation to ACC [Glx] because of the observed ACC phase synchnony within these states. **Figure 6** plots a simple linear regression of the three brain state characteristics and the corrected [Glx] per tissue water. Pearson's correlations are shown in **Table 5**. The only significant correlation was for Pall in State 4 ($p=0.037$). However, following a Bonferroni correction, this significance did not survive muliple comparisons.

a)

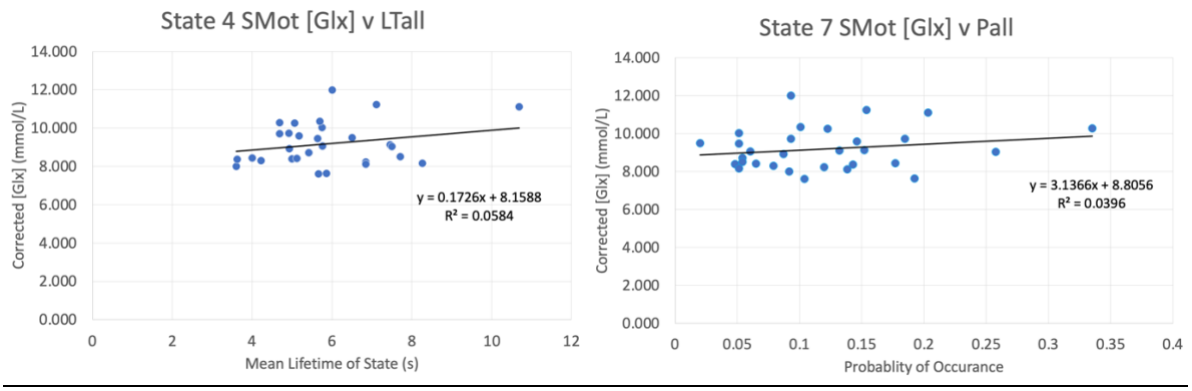

b)

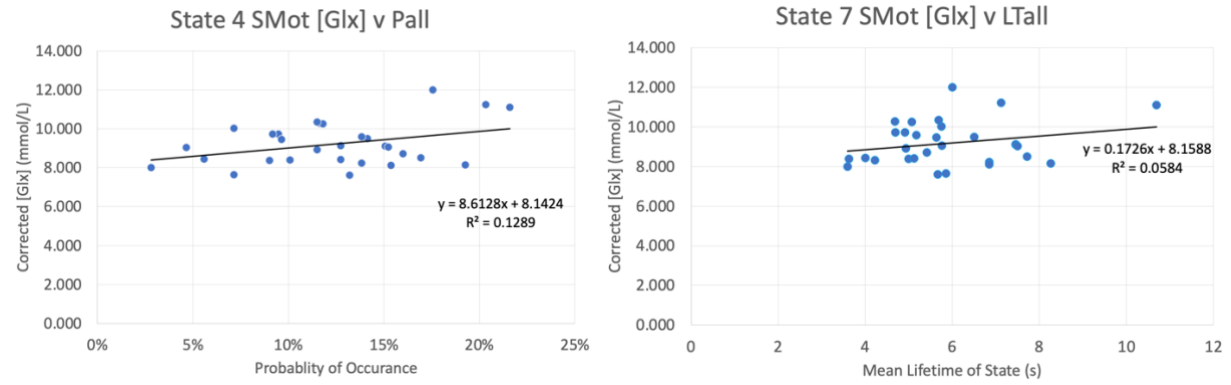

c)

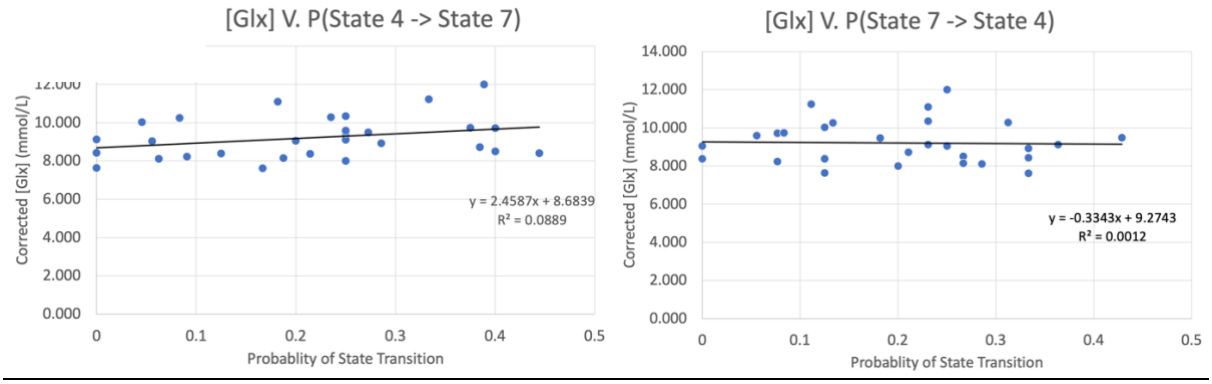

Figure 6: Linear regression between the characteristics (a) Pall, b) LTall, and c) ST) for states dominated by SMot network and corrected Glx concentration.

State Characterisitc		[Glx] per tissue water
Pall Intercingulate State 4	Pearson's r	0.382*
	p-value	0.037
Pall Intercingulate State 7	Pearson's r	0.061
	p-value	0.751
LTall Intercingulate State 4	Pearson's r	0.242
	p-value	0.198
LTall Intercingulate State 7	Pearson's r	0.096
	p-value	0.614
ST Probability Intercingulate State 4 to 7	Pearson's r	0.313
	p-value	0.092
ST Probability Intercingulate State 7 to 4	Pearson's r	-0.012
	p-value	0.951

Table 5: Pearson's Correlation coefficient and p-values for all brain state characteristics with intercingulate states that were in-phase with the ACC; Note: ***** p < .05**, **** p < .01, ******* p < .001, **b** p< .001667 (Bonferroni correction).

The correlation of ACC [Glx] and the state transitions between State 1 to State 2 and State 2 to State 1 was observed, **Table 6.** No significant correlation was made.

State Characterisitc		[Glx] per tissue water
ST Intercingulate State 1 to 2	Pearson's r	0.103
	p-value	0.589
St Intercingulate State 2 to 1	Pearson's r	-0.129
	p-value	0.498

Table 6: Pearson's Correlation coefficient and p-values for the state transition that literature has linked the ACC to play a role in: States 1 to 2 and States 2 to 1; Note: ***** p < .05**, **** p < .01, ******* p < .001, **b** p< .001667 (Bonferroni correction).

3.4.2 Intracingulate

Whilst the inter-ACC network has a single ACC ROI, for the intra-ACC it was worth considering which of our intra-acc seed regions overlaped with the MRS voxel used to measure [Glx]. A visual inspection indicated the regions i6, s6 and s7 were more consistent with the voxel's location. We

hypothesis that it was the properties of states, which incorporate these regions (in phase synchrony with each other and potentially other seeds), that are most likely to show some relationship with cingulate [Glx] as measured with the MRS voxel.

State 1 and State 5 were investigated for this relationship between the characteristics of intracingulate brain states and the corrected [Glx] in the ACC, as these states included two of the three seed regions that overlapped with the MRS voxel

Figure 7 plots simple linear regressions of the three brain state characteristics for States 1 and 5 with the corrected [Glx] per tissue water. No significant correlation between any of the States' brain characterisitics and corrected [Glx] was observed (**Table 6).**

a)

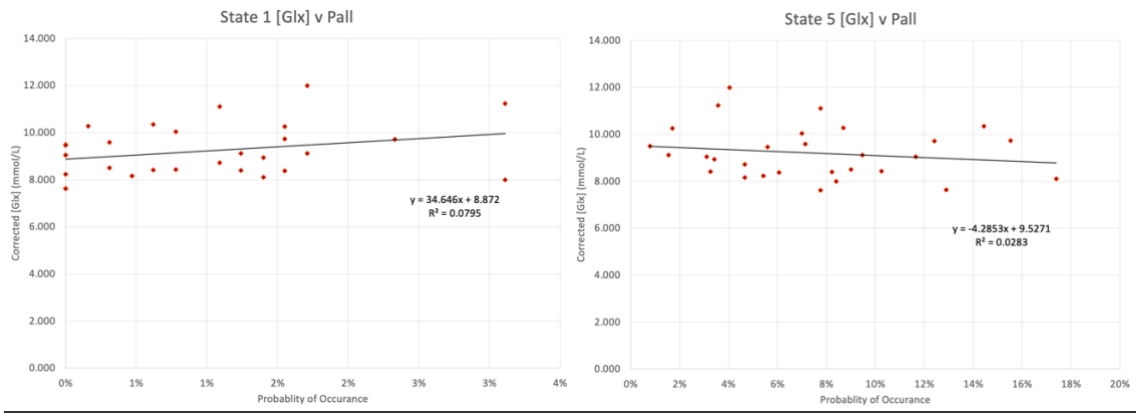

b)

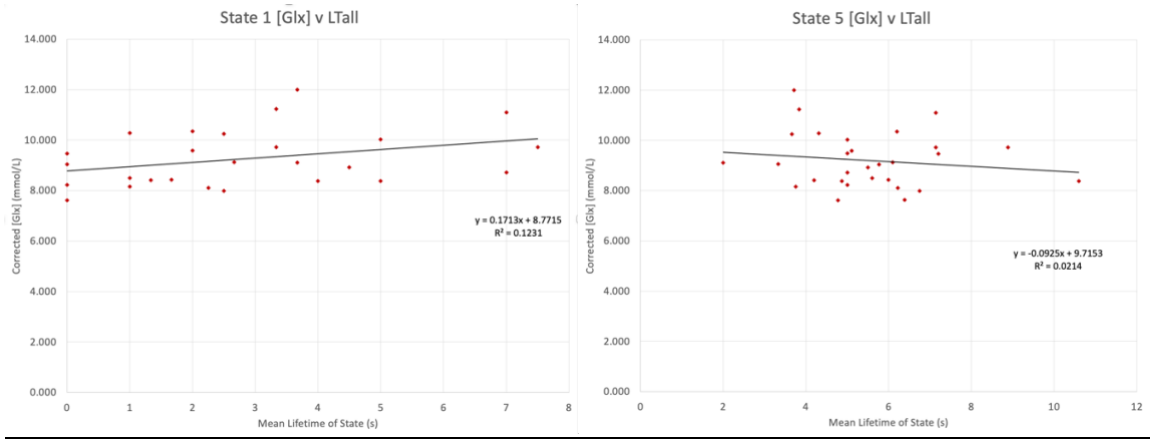

c)

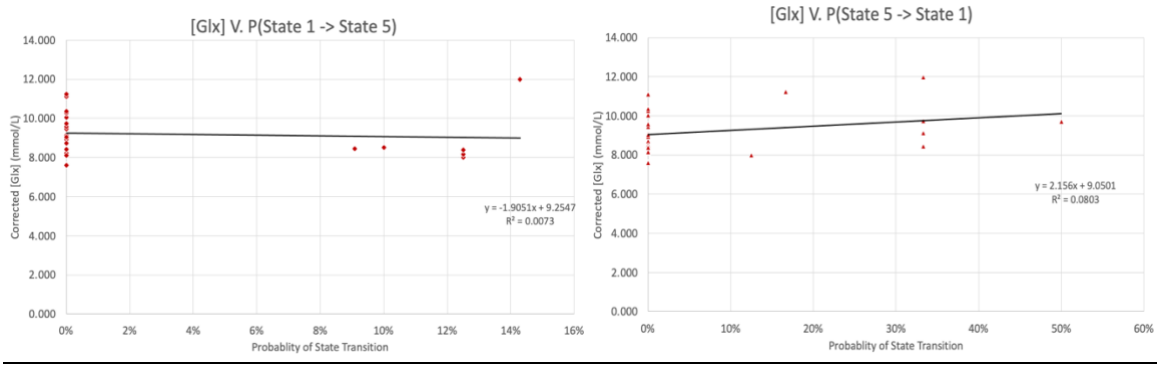

Figure 7: Linear regression between the characteristics (a)Pall, b) LTall, and c) ST) for States 1 and 5 and corrected Glx concentration.

State Characterisitc		[Glx] per tissue water
Pall Intracingulate State 1	Pearson's r	0.297
	p-value	0.111
Pall Intracingulate State 5	Pearson's r	-0.131
	p-value	0.490
LTall Intracingulate State 1	Pearson's r	0.353
	p-value	0.055
LTall Intracingulate State 5	Pearson's r	-0.119
	p-value	0.530
ST Probability Intracingulate State 1 to 5	Pearson's r	-0.071
	p-value	0.711
ST Probability Intracingulate State 5 to 1	Pearson's r	0.293
	p-value	0.116

Table 6: Pearson's Correlation coefficient and p-values for all brain state characteristics in states that had seed activation within the MRS voxel: States 1 and 5; Note: ***** p < .05**,** ****** p < .01, ******* p < .001, **b** p< .001667 (Bonferroni correction)

In addition to our hypothesis-led correlational analyses, which focussed on states where the ACC was a component or where the state incorporated seeds overlapping with the MRS voxel, we carried out an exploratory analysis of the association of [Glx] and the characteristics of the other states identified in the intra- and inter-cingulate network. The Pall and LTall for all intracingulate brain states were compared to the corrected [Glx] (**Table 7 and 8)**. Prior to multiple comparisons, significant correlations were found for Pall in State 2 (p=0.049) and State 3 (p=0.022). However, no statistically significant findings were observed for the lifetime characteristic.

State Characterisitc		[Glx] per tissue water
Pall Intracingulate State 1	Pearson's r	0.297
	p-value	0.111
Pall Intracingulate State 2	Pearson's r	0.363
	p-value	0.049*
Pall Intracingulate State 3	Pearson's r	0.418
	p-value	0.022*
Pall Intracingulate State 4	Pearson's r	-0.034
	p-value	0.858
Pall Intracingulate State 5	Pearson's r	-0.131
	p-value	0.490
Pall Intracingulate State 6	Pearson's r	0.110
	p-value	0.562
Pall Intracingulate State 7	Pearson's r	-0.293
	p-value	0.117
Pall Intracingulate State 8	Pearson's r	-0.024
	p-value	0.901
Pall Intracingulate State 9	Pearson's r	-0.168
	p-value	0.376

Table 7: Pearson's Correlation coefficient and p-values for all Pall of each intracingulate state; Note: ***** $p < .05$**,** ****** $p < .01$, ******* $p < .001$, **b** $p < .001667$ (Bonferroni correction)

State Characterisitc		[Glx] per tissue water
LTall Intracingulate State 1	Pearson's r	0.353
	p-value	0.055
LTall Intracingulate State 2	Pearson's r	0.181
	p-value	0.339
LTall Intracingulate State 3	Pearson's r	0.308
	p-value	0.098
LTall Intracingulate State 4	Pearson's r	-0.133
	p-value	0.482
LTall Intracingulate State 5	Pearson's r	-0.119
	p-value	0.530
LTall Intracingulate State 6	Pearson's r	0.130
	p-value	0.494
LTall Intracingulate State 7	Pearson's r	-0.177
	p-value	0.350
LTall Intracingulate State 8	Pearson's r	0.010
	p-value	0.959
LTall Intracingulate State 9	Pearson's r	-0.006
	p-value	0.973

Table 8: Pearson's Correlation coefficient and p-values for all LTall of each intracingulate state; Note: ***** p < .05**,** ****** p < .01, ******* p < .001, **b** p< .001667 (Bonferroni correction)

4. Discussion

The present study aimed to identify broad distributed brain networks that transiently include the ACC (intercingulate), and to determine the degree to which discrete states, identified as patterns of dynamic connectivity, could be identified within the ACC (intracingulate). Additionally, the present study aimed to investigate whether the dynamic characteristics of any such networks or states identified could be correlated to individual differences in cingulate glutamate concentrations, as measured by [Glx] in the ACC. The three salient findings or outcomes can be summarized as below:

(a) this was the first study to successfully use the ACC parcellation methodology developed by Margulies et al. (2007) to observe dynamic brain states in the subregions of a particular brain structure

(b) no statistically significant relationship was observed between individual differences of [Glx] in the ACC and intercingulate brain regions

(c) no statistically significant relationship was observed between individual differences of [Glx] in the ACC and intracingulate brain regions

4.1 MRS Glutamate Concentration

In the present study, we found the average concentration for the corrected [Glx] in the ACC MRS voxel to be 9.56 mmol/L. This concentration, however, differs from the corrected [Glx] values more commonly reported in the literature. This discrepancy could be accounted for by the method used for the concentration correction; in this study [Glx] was corrected to tissue water, while a significant proportion of the literature corrects to tissue creatine. Creatine (Cr) is traditionally used in MRS neuroimaging to correct for metabolite concentrations by establishing a standardized ratio for the metabolite, such as Glu, to be compared against. However, more recently, the use of creatine to correct metabolite concentrations has been scrutinized, as the concentration of creatine itself in an individual's brain is highly variable. The use of tissue water for these corrected concentrations has become more popular, despite its large volume in brain tissue, as the concentration of water is more stable. So, the difference in standard against which the correction of the [Glu] was made likely accounts for the observed difference in the corrected [Glx] value.

Furthermore, this is the first study, to our knowledge, that calculates the corrected [Glx] in the ACC, with tissue water as the standard, using a 3T scanner. That is, if this study had adopted the concentration of creatine as the standard to find the corrected [Glx] using a 3T scanner, we would have identified a ratio of 1.49, which would have been broadly consistent with the ratio of 1.7 found by Fayed

et al. (2011) using a 1.5T scanner. The difference between the reported ratios from the present study and from Fayed et al. (2011) can be accounted for by the difference in scanner used. Findings from Kim et al. (2006) suggest that as the signal-to-noise ratio increases with higher Tesla scanners, metabolite concentration measurements reduce slightly. This aligns with the observation above, such that using a 3T scanner we found a ratio of 1.49, while using a 1.5T scanner Fayed et al. (2011) found a higher ratio of 1.7.

For the MRS glutamate concentration data set, collected from the group of 30 healthy subjects, one outlier for the [Glx] in the ACC was identified. Similarly, in a previous study by Gallinat et al. (2016) two outliers were identified in a healthy population of 30. Together, these findings seem to indicate that within a healthy population, the [Glx] in the ACC is similar between individuals. Furthermore, this suggests that potential differences between [Glx] in a healthy population compared to a diseased population is worth considering. Indeed, in patients with early psychosis, lower [Glx] was observed in comparison to the heathy population (Godlewska et al., 2021). This decrease in [Glx] lead to a significant correlation between ACC glutamate levels and performance on cognitive assessments (Godlewska et al., 2021).

4.2 Intercingulate Brain States

4.2.1 dFC of Intercingulate

ACC phase synchrony with known functional networks was observed in two of the seven identified intercingulate brain states, namely States 4 and 7. As expected, in both States 4 and 7, the ACC was in-phase with the somato-motor network (SMot), which supports previous findings that the ACC is reciprocally connected to the sensory and motor regions of the brain (Goulden et al., 2014). The ACC, however, showed no synchrony with the DMN and the FrPar. This was also expected, as there should be no phase synchrony between the ACC and these networks, because the ACC is involved in the salience network. These findings are consistent with the ideas from Goulden et al. (2014) that the salience network drives and regulates the ST between the DMN and FrPar. This is further supported by Sridharan et al. (2007), which found for the salience network, the right fronto-insular cortex and the ACC during simultaneous activity in the FrPar and deactivation of the DMN.

4.2.2 [Glx] effect on Intercingulate State

Following multiple comparison corrections, [Glx] was not significantly associated with state characteristics (i.e., probability of occurrence (Pall), mean lifetime (LTall) and probability of state transitions (ST)) in intercingulate brain states dominated by the SMoT. For the multiple comparison corrections, the Bonferroni correction was used to control for the risk of Type I error or false-positive error. As the correlation between the [Glx] in the ACC and Pall in brain State 4 [Glx] was not significant following the Bonferroni correction, it should be attributed to a Type I error, and thus nullified.

Although both intercingulate brain States 4 and 7 were dominated by the same network (SMot), the overlapping synchronous networks varied between the two. State 4 was in synchrony with the ventral attention Yeo network (VenATT), while State 7 was in synchrony with visual Yeo network (Vis). The ventral attention network is responsible for attention, which is promoted through detection of salient events (Menon and Uddin, 2010). The ACC, a part of the salience network, has been shown to play a role in saliency detection of salient stimuli/events (Menon and Uddin, 2010). This indicates that both the salience network ACC and ventral attention network are intertwined with each other. The language network and visual network are also related to one another. In a study by Hutton et al. (2019) observing different FC patterns in visual and language network in preschooled-age children through different mediums of learning, it was discovered that when children use illustrated books, the visual network and language networks are integrated. Through knowledge of these intertwined networks, most likely, this is the reason why there were different brain characteristics for two different states that were dominated by the same SMoT.

Additionally, States 1 and 2, which were dominated by the DMN and FrPar, were used to determine if there was a relationship between probability of state transitions from the DMN to the FrPar, as well as from the FrPar to the DMN and [Glx] in the ACC. Previous research has demonstrated that the ACC is involved in the transition between these two states; however, no significant correlation was observed between ST and [Glx] in the ACC. This was surprising as it indicates that, contrary to our hypothesis, the [Glu] in the ACC may not influence the dFC of intercingulate networks corresponding with the ACC.

4.3 Intracingulate States

4.3.1 dFC of Intracingulate

When examining the phase synchrony of intracingulate ACC seeds, nine brain states were identified for the resting-state ACC. Of these nine brain states identified in the ACC, eight showed periods of phase synchrony with a varied subset of the 32 ROIs or ACC seeds. State 9, however, did

not show phase synchrony with any of the 32 ACC seeds. One possible explanation for the lack of phase synchrony might be that State 9 only shows synchrony with regions of the ACC not within the 32 ACC seeds or ROI spheres. Alternatively, it may be that State 9 does not show phase synchrony anywhere in the ACC. Meanwhile, intracingulate States 1 and 5 showed activation in at least two of the three ACC seeds (s6, s7, i6) in the same hemisphere located within the MRS voxel, and as such qualified for further analysis. According to Margulies et al. (2007), the rostral seeds, s6 and s7, negatively predicted activity in brain regions linked to the attentional and sensorimotor networks, while i6 were positively correlated with the paralimbic and limbic regions. Seeds s6+ and s7+ were in-phase and localized in the MRS voxel during State 1. In State 5, the ACC seeds which showed phase-synchrony were s6- and s7-. Therefore, the inference can be made that the s6 and s7 in the present study was dynamically coupled with the attentional and sensorimotor networks

4.3.2 [Glx] effect on IntraACC States

When intraACC states with synchronous seeds located within the MRS voxel were correlated separately with corrected [Glx] in the ACC to observe whether there is a relationship, there were no significant findings. Additionally, in observing the relationship of all intraACC states and [Glx], we found evidence that glutamate was significantly related to dFC of the intracingulate. The ACC is a major hub for regulation, heavily interconnected and many functional distinct regions within the ACC are implicated in many functions. Moreover, these were interesting results as Glu is a major excitatory transmitter of the ACC. Since the ACC also is known to contain a lot of overall Glu, it was expected that [Glx] would have some form of a relationship with intraACC states and their characteristics. Perhaps, Glu does not have a relationship with intraACC states, but rather other neurotransmitters (i.e., GABA) or neuromodulators (i.e., serotonin and dopamine) abundant in the anterior cingulate cortex has an effect on intraACC states.

4.4 Parcellation of ACC for dFC

As mentioned in the previous section, our study set forth the novel possibility to parcellate the ACC into smaller subregions to study phase synchrony among the rostral, caudal, and subgenual subunits of the ACC. No prior study, to our knowledge, has established a protocol to observe the dynamical intracingulate brain states, as well as the characteristics of these brain states within ACC subregions. While we found strong evidence in favor of parcellation, a confirmatory study would be needed to replicate this protocol and confirm evidence for the successful observation of dynamical intracingulate brain states. Although we applied this parcellation method only to the ACC in this study,

the same methodology could be used to parcellate the entire cingulate cortex to include the posterior cingulate cortex, as well as other brain subregions when studying dFC.

4.5 Limitations

Two significant limitations to this study are as listed: Firstly, within the protocol the rsfMRI and MRS scans are taken sequentially rather than simultaneously. However, in a recent study by Betina et al. (2017), a new protocol was developed to investigate FC and metabolite concentrations through simultaneous acquisition of fMRI and MRS data. Although Betina et al. (2017) studied metabolites in the occipital lobe, the protocol for simultaneous acquisition of imaging data allows the same T_R for MRS and rsfMRI to be used. This, in turn, provides more direct and accurate insight into the correlation between metabolite concentrations and brain state characteristics or dynamical brain states because there would be more measurements of Glx "in-real time," allow for direct inferences to be made regarding dFC and [Glx]. Secondly, for the investigation of the dFC of intracingulate brain states, only six of the 32 ACC seeds or ROIs were located within the MRS voxel. If the MRS voxel had been shifted to include a higher number of ACC seeds or ROIs, we would have been able to produce findings with higher accuracy by directly correlating [Glx] to functional connectivity within the ACC brain region.

4.6 Further Research

Although we did not find evidence in support of our hypothesis that [Glx] in the ACC is related to some core behavioural characteristics of brain states of healthy individuals; further investigation into other metabolites in the ACC, which may influence brain states, is warranted. Serotonin (5-HT), specifically, modulates excitatory transmission in the central nervous system. Continued research to determine whether [5-HT] in the ACC shows an observable correlation to brain state characteristics at resting-state. To pursue this, a modified version of the protocol included in this study could be used.

Another direction for future research is to utilize the same protocol included in this study with the addition of a second cohort (n=30) of subjects with a diagnosis of various psychiatric illnesses such as schizophrenia or major depression disorder. The aim for this would be to determine how [Glx] in the ACC may influence brain states in subjects with different psychiatric illness. This suggestion for future research stems from the observation that there is not much variation in the [Glx] of healthy individuals. It is worth investigating if is more variation in subjects with mental illness, and perhaps such variations might impact the brain states of those patients differently than in a healthy population.

4.7 Conclusion

In review, the present study provided evidence for novel methodologies in multi-modal neuroimaging studies. Firstly, this study was the first, to our knowledge, to demonstrate the possibility of using ACC parcellation methodology to observe dynamic brain states. The success of the parcellation of the ACC to observe subregion connectivity through MRS, suggest that the parcellation methodology might provide an avenue to future understanding of the psychopathologies of psychiatric disorders. Secondly, this study was the first to document corrected [Glx] to tissue water in the ACC using a 3T scanner. However, contrary to our hypotheses, we did not observe correlations between varying [Glx] in the ACC and both intercingulate and intracingulate brain states.

5. Acknowledgments

I would like to thank Dr. Owen O'Daly (Centre of Neuroimaging Sciences, Institute of Psychiatry, Psychology, and Neuroscience, King's College London) for your expertise on neuroimaging, and mentoring me on my academic development over the course of the year.

I would also like to thank Marie-Stephanie Cahart for all the dFC help along the way and wish her good luck on her academic endeavours.

Lastly, I would like to thank my family for encouraging me to pursue my studies abroad.

6. References

Aedo-Jury, F., Schwalm, M., Hamzehpour, L., & Stroh, A. (2020). Brain states govern the spatio-temporal dynamics of resting-state functional connectivity. *ELife*, *9*, e53186. https://doi.org/10.7554/eLife.53186

Alexander, L., Jelen, L., Mehta, M., & Young, A. (2021). The anterior cingulate cortex as a key locus of ketamine's antidepressant action. *Neuroscience & Biobehavioral Reviews*, *127*. https://doi.org/10.1016/j.neubiorev.2021.05.003

Alger, J. R. (2009). Magnetic Resonance Spectroscopy. In *Encyclopedia of Neuroscience* (pp. 601–607). Academic Press. https://www.sciencedirect.com/science/article/pii/B9780080450469003004

Belov Kirdajova, D., Kriska, J., Tureckova, J., & Anderova, M. (2020). Ischemia-Triggered Glutamate Excitotoxicity From the Perspective of Glial Cells. *Frontiers in Cellular Neuroscience*, *14*. https://www.frontiersin.org/article/10.3389/fncel.2020.00051

Berman, R. M., Cappiello, A., Anand, A., Oren, D. A., Heninger, G. R., Charney, D. S., & Krystal, J. H. (2000). Antidepressant effects of ketamine in depressed patients. *Biological Psychiatry*, *47*(4), 351–354. https://doi.org/10.1016/S0006-3223(99)00230-9

Betina Ip, I., Berrington, A., Hess, A. T., Parker, A. J., Emir, U. E., & Bridge, H. (2017). Combined fMRI-MRS acquires simultaneous glutamate and BOLD-fMRI signals in the human brain. *Neuroimage*, *155*, 113–119. https://doi.org/10.1016/j.neuroimage.2017.04.030

Brett, M., Anton, J.-L., Valabregue, R., & Poline, J.-B. (n.d.). *Region of interest analysis using an SPM toolbox*. 1.

Cabral, J. (2021, June 5). *Joana Cabral—LEiDA - Leading Eigenvector Dynamics Analysis*. https://sites.google.com/site/cvjoanacabral/codes/leida-leading-eigenvector-dynamics-analysis

Cabral, J., Vidaurre, D., Marques, P., Magalhães, R., Silva Moreira, P., Miguel Soares, J., Deco, G., Sousa, N., & Kringelbach, M. L. (2017). Cognitive performance in healthy older adults relates to spontaneous switching between states of functional connectivity during rest. *Scientific Reports*, *7*, 5135. https://doi.org/10.1038/s41598-017-05425-7

Carriedo, S. G., Yin, H. Z., & Weiss, J. H. (1996). Motor Neurons Are Selectively Vulnerable to AMPA/Kainate Receptor-Mediated Injury In Vitro. *Journal of Neuroscience*, *16*(13), 4069–4079. https://doi.org/10.1523/JNEUROSCI.16-13-04069.1996

Cosgrove, J., & Newell, T. G. (1991). Recovery of neuropsychological functions during reduction in use of phencyclidine. *Journal of Clinical Psychology*, *47*(1), 159–169. https://doi.org/10.1002/1097-4679(199101)47:1<159::AID-JCLP2270470125>3.0.CO;2-O

Cruzat, V., Macedo Rogero, M., Noel Keane, K., Curi, R., & Newsholme, P. (2018). Glutamine: Metabolism and Immune Function, Supplementation and Clinical Translation. *Nutrients*, *10*(11), 1564. https://doi.org/10.3390/nu10111564

Deakin, J. F. W., Lees, J., McKie, S., Hallak, J. E. C., Williams, S. R., & Dursun, S. M. (2008). Glutamate and the Neural Basis of the Subjective Effects of Ketamine: A Pharmaco–Magnetic Resonance

Imaging Study. *Archives of General Psychiatry*, *65*(2), 154–164. https://doi.org/10.1001/archgenpsychiatry.2007.37

Deco, G., Cruzat, J., Cabral, J., Tagliazucchi, E., Laufs, H., Logothetis, N. K., & Kringelbach, M. (2019). Awakening: Predicting external stimulation to force transitions between different brain states. *Proceedings of the National Academy of Sciences*, *116*(36), 18088–18097. https://doi.org/10.1073/pnas.1905534116

Eickhoff, S., & Muller, V. (2015). Functional Connectivity. In *Brain Mapping: An Encyclopedic Reference* (Vol. 2, pp. 187–201). Elsevier's.

Falkenberg, L. E., Westerhausen, R., Craven, A. R., Johnsen, E., Kroken, R. A., L⊘berg, E.-M., Specht, K., & Hugdahl, K. (2014). Impact of glutamate levels on neuronal response and cognitive abilities in schizophrenia. *NeuroImage: Clinical*, *4*, 576–584. https://doi.org/10.1016/j.nicl.2014.03.014

Farinha, M., Amado, C., Morgado, P., & Cabral, J. (2022). Increased Excursions to Functional Networks in Schizophrenia in the Absence of Task. *Frontiers in Neuroscience*, *16*. https://www.frontiersin.org/articles/10.3389/fnins.2022.821179

Fayed, N., Modrego, P. J., Rojas-Salinas, G., & Aguilar, K. (2011). Brain Glutamate Levels Are Decreased in Alzheimer's Disease: A Magnetic Resonance Spectroscopy Study. *American Journal of Alzheimer's Disease & Other Dementias®*, *26*(6), 450–456. https://doi.org/10.1177/1533317511421780

Friston, K. J. (1994). Functional and effective connectivity in neuroimaging: A synthesis. *Human Brain Mapping*, *2*(1–2), 56–78. https://doi.org/10.1002/hbm.460020107

Gallinat, J., McMahon, K., Kühn, S., Schubert, F., & Schaefer, M. (2016). Cross-sectional Study of Glutamate in the Anterior Cingulate and Hippocampus in Schizophrenia. *Schizophrenia Bulletin*, *42*(2), 425–433. https://doi.org/10.1093/schbul/sbv124

Gasparovic, C., Song, T., Devier, D., Bockholt, H. J., Caprihan, A., Mullins, P. G., Posse, S., Jung, R. E., & Morrison, L. A. (2006). Use of tissue water as a concentration reference for proton spectroscopic imaging. *Magnetic Resonance in Medicine*, *55*(6), 1219–1226. https://doi.org/10.1002/mrm.20901

Gaudet, I., Hüsser, A., Vannasing, P., & Gallagher, A. (2020). Functional Brain Connectivity of Language Functions in Children Revealed by EEG and MEG: A Systematic Review. *Frontiers in Human Neuroscience*, *14*. https://www.frontiersin.org/articles/10.3389/fnhum.2020.00062

Glutamate and functional connectivity—Support for the excitatory-inhibitory imbalance hypothesis in autism spectrum disorders | Elsevier Enhanced Reader. (n.d.). https://doi.org/10.1016/j.pscychresns.2021.111302

Goulden, N., Khusnulina, A., Davis, N. J., Bracewell, R. M., Bokde, A. L., McNulty, J. P., & Mullins, P. G. (2014a). The salience network is responsible for switching between the default mode network and the central executive network: Replication from DCM. *NeuroImage*, *99*, 180–190. https://doi.org/10.1016/j.neuroimage.2014.05.052

Goulden, N., Khusnulina, A., Davis, N. J., Bracewell, R. M., Bokde, A. L., McNulty, J. P., & Mullins, P. G. (2014b). The salience network is responsible for switching between the default mode network and

the central executive network: Replication from DCM. *NeuroImage*, *99*, 180–190. https://doi.org/10.1016/j.neuroimage.2014.05.052

Govindaraju, V., Young, K., & Maudsley, A. A. (2000). Proton NMR chemical shifts and coupling constants for brain metabolites. *NMR in Biomedicine*, *13*(3), 129–153. https://doi.org/10.1002/1099-1492(200005)13:3<129::AID-NBM619>3.0.CO;2-V

Guo, K., Benson, P. J., & Blakemore, C. (2004). Pattern motion is present in V1 of awake but not anaesthetized monkeys. *The European Journal of Neuroscience*, *19*(4), 1055–1066. https://doi.org/10.1111/j.1460-9568.2004.03212.x

Hancock, F., Cabral, J., Luppi, A. I., Rosas, F. E., Mediano, P. A. M., Dipasquale, O., & Turkheimer, F. E. (2022). *Metastability, fractal scaling, and synergistic information processing: What phase relationships reveal about intrinsic brain activity* [Preprint]. Neuroscience. https://doi.org/10.1101/2022.01.17.476583

Hillman, E. M. C. (2014). Coupling Mechanism and Significance of the BOLD Signal: A Status Report. *Annual Review of Neuroscience*, *37*, 161–181. https://doi.org/10.1146/annurev-neuro-071013-014111

Hindriks, R., Adhikari, M. H., Murayama, Y., Ganzetti, M., Mantini, D., Logothetis, N. K., & Deco, G. (2016). Can sliding-window correlations reveal dynamic functional connectivity in resting-state fMRI? *Neuroimage*, *127*, 242–256. https://doi.org/10.1016/j.neuroimage.2015.11.055

Honey, C. J., Sporns, O., Cammoun, L., Gigandet, X., Thiran, J. P., Meuli, R., & Hagmann, P. (2009). Predicting human resting-state functional connectivity from structural connectivity. *Proceedings of the National Academy of Sciences*, *106*(6), 2035–2040. https://doi.org/10.1073/pnas.0811168106

Hutchison, R. M., Womelsdorf, T., Allen, E. A., Bandettini, P. A., Calhoun, V. D., Corbetta, M., Della Penna, S., Duyn, J. H., Glover, G. H., Gonzalez-Castillo, J., Handwerker, D. A., Keilholz, S., Kiviniemi, V., Leopold, D. A., de Pasquale, F., Sporns, O., Walter, M., & Chang, C. (2013). Dynamic functional connectivity: Promise, issues, and interpretations. *NeuroImage*, *80*, 360–378. https://doi.org/10.1016/j.neuroimage.2013.05.079

Jamovi Project. (2022). *Jamovi* (2.3). Jamovi. https://www.jamovi.org/

Javitt, D. C. (2004). Glutamate as a therapeutic target in psychiatric disorders. *Molecular Psychiatry*, *9*(11), 984–997. https://doi.org/10.1038/sj.mp.4001551

Jing, H., Cheng, Y., Li, S., & Zhang, G. (2000). [Effects of glutamate and glutamine on learning and memory of rats]. *Wei Sheng Yan Jiu = Journal of Hygiene Research*, *29*(1), 40–42.

Jones, B. F., Groenewegen, H. J., & Witter, M. P. (2005). Intrinsic connections of the cingulate cortex in the rat suggest the existence of multiple functionally segregated networks. *Neuroscience*, *133*(1), 193–207. https://doi.org/10.1016/j.neuroscience.2005.01.063

Jumah, F. R., & Dossani, R. H. (2022). Neuroanatomy, Cingulate Cortex. In *StatPearls*. StatPearls Publishing. http://www.ncbi.nlm.nih.gov/books/NBK537077/

Kim, J., Chang, K.-H., Na, D. G., Song, I. C., Kim, S. J., Kwon, B. J., & Han, M. H. (2006). Comparison of 1.5T and 3T 1H MR Spectroscopy for Human Brain Tumors. *Korean Journal of Radiology*, *7*(3), 156–161. https://doi.org/10.3348/kjr.2006.7.3.156

Kringelbach, M. L., & Deco, G. (2020). Brain States and Transitions: Insights from Computational Neuroscience. *Cell Reports*, *32*(10), 108128. https://doi.org/10.1016/j.celrep.2020.108128

Lee, D., Lee, J., Namkoong, K., & Jung, Y.-C. (2018). Subregions of the Anterior Cingulate Cortex Form Distinct Functional Connectivity Patterns in Young Males With Internet Gaming Disorder With Comorbid Depression. *Frontiers in Psychiatry*, *9*, 380. https://doi.org/10.3389/fpsyt.2018.00380

Lewerenz, J., & Maher, P. (2015). Chronic Glutamate Toxicity in Neurodegenerative Diseases—What is the Evidence? *Frontiers in Neuroscience*, *9*. https://www.frontiersin.org/articles/10.3389/fnins.2015.00469

Li, C.-T., Yang, K.-C., & Lin, W.-C. (2019). Glutamatergic Dysfunction and Glutamatergic Compounds for Major Psychiatric Disorders: Evidence From Clinical Neuroimaging Studies. *Frontiers in Psychiatry*, *9*. https://www.frontiersin.org/article/10.3389/fpsyt.2018.00767

Lv, H., Wang, Z., Tong, E., Williams, L. M., Zaharchuk, G., Zeineh, M., Goldstein-Piekarski, A. N., Ball, T. M., Liao, C., & Wintermark, M. (2018). Resting-State Functional MRI: Everything That Nonexperts Have Always Wanted to Know. *American Journal of Neuroradiology*. https://doi.org/10.3174/ajnr.A5527

Maddock, R. J., Caton, M. D., & Ragland, J. D. (2018). Estimating Glutamate and Glx from GABA-Optimized MEGA-PRESS: Off-Resonance but not Difference Spectra Values Correspond to PRESS Values. *Psychiatry Research. Neuroimaging*, *279*, 22–30. https://doi.org/10.1016/j.pscychresns.2018.07.003

Margulies, D. S., Kelly, A. M. C., Uddin, L. Q., Biswal, B. B., Castellanos, F. X., & Milham, M. P. (2007). Mapping the functional connectivity of anterior cingulate cortex. *NeuroImage*, *37*(2), 579–588. https://doi.org/10.1016/j.neuroimage.2007.05.019

Marsman, A., van den Heuvel, M. P., Klomp, D. W. J., Kahn, R. S., Luijten, P. R., & Hulshoff Pol, H. E. (2013). Glutamate in Schizophrenia: A Focused Review and Meta-Analysis of 1H-MRS Studies. *Schizophrenia Bulletin*, *39*(1), 120–129. https://doi.org/10.1093/schbul/sbr069

Matosin, N., Fernandez-Enright, F., Frank, E., Deng, C., Wong, J., Huang, X.-F., & Newell, K. A. (2014). Metabotropic glutamate receptor mGluR2/3 and mGluR5 binding in the anterior cingulate cortex in psychotic and nonpsychotic depression, bipolar disorder and schizophrenia: Implications for novel mGluR-based therapeutics. *Journal of Psychiatry and Neuroscience*, *39*(6), 407–416. https://doi.org/10.1503/jpn.130242

Mattson, M. P., Cheng, B., Davis, D., Bryant, K., Lieberburg, I., & Rydel, R. E. (1992). Beta-Amyloid peptides destabilize calcium homeostasis and render human cortical neurons vulnerable to excitotoxicity. *Journal of Neuroscience*, *12*(2), 376–389. https://doi.org/10.1523/JNEUROSCI.12-02-00376.1992

McOmish, C. E., Pavey, G., Gibbons, A., Hopper, S., Udawela, M., Scarr, E., & Dean, B. (2016). Lower [3H]LY341495 binding to mGlu2/3 receptors in the anterior cingulate of subjects with major depressive disorder but not bipolar disorder or schizophrenia. *Journal of Affective Disorders*, *190*, 241–248. https://doi.org/10.1016/j.jad.2015.10.004

Ménard, C., & Quirion, R. (2012). Group 1 Metabotropic Glutamate Receptor Function and Its Regulation of Learning and Memory in the Aging Brain. *Frontiers in Pharmacology*, *3*. https://www.frontiersin.org/article/10.3389/fphar.2012.00182

Menon, S. S., & Krishnamurthy, K. (2019). A Comparison of Static and Dynamic Functional Connectivities for Identifying Subjects and Biological Sex Using Intrinsic Individual Brain Connectivity. *Scientific Reports*, *9*(1), 5729. https://doi.org/10.1038/s41598-019-42090-4

Menon, V., & Uddin, L. Q. (2010). Saliency, switching, attention and control: A network model of insula function. *Brain Structure and Function*, *214*(5), 655–667. https://doi.org/10.1007/s00429-010-0262-0

Mikkelsen, M., Rimbault, D. L., Barker, P. B., Bhattacharyya, P. K., Brix, M. K., Buur, P. F., Cecil, K. M., Chan, K. L., Chen, D. Y.-T., Craven, A. R., Cuypers, K., Dacko, M., Duncan, N. W., Dydak, U., Edmondson, D. A., Ende, G., Ersland, L., Forbes, M. A., Gao, F., … Edden, R. A. E. (2019). Big GABA II: Water-Referenced Edited MR Spectroscopy at 25 Research Sites. *NeuroImage*, *191*, 537–548. https://doi.org/10.1016/j.neuroimage.2019.02.059

Modi, S., Rana, P., Kaur, P., Rani, N., & Khushu, S. (2014). Glutamate level in anterior cingulate predicts anxiety in healthy humans: A magnetic resonance spectroscopy study. *Psychiatry Research: Neuroimaging*, *224*(1), 34–41. https://doi.org/10.1016/j.pscychresns.2014.03.001

Near, J., Harris, A. D., Juchem, C., Kreis, R., Marjańska, M., Öz, G., Slotboom, J., Wilson, M., & Gasparovic, C. (2021). Preprocessing, analysis and quantification in single-voxel magnetic resonance spectroscopy: Experts' consensus recommendations. *NMR in Biomedicine*, *34*(5), e4257. https://doi.org/10.1002/nbm.4257

Palomero-Gallagher, N., Mohlberg, H., Zilles, K., & Vogt, B. (2008). Cytology and receptor architecture of human anterior cingulate cortex. *Journal of Comparative Neurology*, *508*(6), 906–926. https://doi.org/10.1002/cne.21684

Parvizi, J., Van Hoesen, G. W., Buckwalter, J., & Damasio, A. (2006). Neural connections of the posteromedial cortex in the macaque. *Proceedings of the National Academy of Sciences*, *103*(5), 1563–1568. https://doi.org/10.1073/pnas.0507729103

Petrides, M., & Pandya, D. N. (1994). Comparative architectonic analysis of the human and the macaque frontal cortex. *Handbook of Neuropsychology*, 17–58.

PII: S0006-3223(99)00230-9 | Elsevier Enhanced Reader. (n.d.). https://doi.org/10.1016/S0006-3223(99)00230-9

Provencher, S. W. (1993). Estimation of metabolite concentrations from localized in vivo proton NMR spectra. *Magnetic Resonance in Medicine*, *30*(6), 672–679. https://doi.org/10.1002/mrm.1910300604

Provencher, S. W. (2001). Automatic quantitation of localized in vivo 1H spectra with LCModel. *NMR in Biomedicine*, *14*(4), 260–264. https://doi.org/10.1002/nbm.698

R Core Team. (2021). *R: A language and environment for statistical* (4.1). https://cran.r-project.org/

Ramadan, S., Lin, A., & Stanwell, P. (2013). Glutamate and Glutamine: A Review of In Vivo MRS in the Human Brain. *NMR in Biomedicine*, *26*(12), 10.1002/nbm.3045. https://doi.org/10.1002/nbm.3045

Sendi, M. S. E., Zendehrouh, E., Sui, J., Fu, Z., Zhi, D., Lv, L., Ma, X., Ke, Q., Li, X., Wang, C., Abbott, C. C., Turner, J. A., Miller, R. L., & Calhoun, V. D. (2021). Abnormal Dynamic Functional Network Connectivity Estimated from Default Mode Network Predicts Symptom Severity in Major Depressive Disorder. *Brain Connectivity*. https://doi.org/10.1089/brain.2020.0748

Siegel-Ramsay, J. E., Romaniuk, L., Whalley, H. C., Roberts, N., Branigan, H., Stanfield, A. C., Lawrie, S. M., & Dauvermann, M. R. (2021). Glutamate and functional connectivity—Support for the excitatory-inhibitory imbalance hypothesis in autism spectrum disorders. *Psychiatry Research: Neuroimaging*, *313*, 111302. https://doi.org/10.1016/j.pscychresns.2021.111302

Srinivasan, R., Cunningham, C., Chen, A., Vigneron, D., Hurd, R., Nelson, S., & Pelletier, D. (2006). TE-Averaged two-dimensional proton spectroscopic imaging of glutamate at 3 T. *NeuroImage*, *30*(4), 1171–1178. https://doi.org/10.1016/j.neuroimage.2005.10.048

Stevens, F. L., Hurley, R. A., Taber, K. H., Hurley, R. A., Hayman, L. A., & Taber, K. H. (2011). Anterior Cingulate Cortex: Unique Role in Cognition and Emotion. *The Journal of Neuropsychiatry and Clinical Neurosciences*, *23*(2), 121–125. https://doi.org/10.1176/jnp.23.2.jnp121

Taghia, J., Cai, W., Ryali, S., Kochalka, J., Nicholas, J., Chen, T., & Menon, V. (2018). Uncovering hidden brain state dynamics that regulate performance and decision-making during cognition. *Nature Communications*, *9*(1), 2505. https://doi.org/10.1038/s41467-018-04723-6

Tognarelli, J. M., Dawood, M., Shariff, M. I. F., Grover, V. P. B., Crossey, M. M. E., Cox, I. J., Taylor-Robinson, S. D., & McPhail, M. J. W. (2015). Magnetic Resonance Spectroscopy: Principles and Techniques: Lessons for Clinicians. *Journal of Clinical and Experimental Hepatology*, *5*(4), 320–328. https://doi.org/10.1016/j.jceh.2015.10.006

Tong, Y., Hocke, L. M., & Frederick, B. deB. (2014). Short Repetition Time Multiband Echo-Planar Imaging with Simultaneous Pulse Recording Allows Dynamic Imaging of the Cardiac Pulsation Signal. *Magnetic Resonance in Medicine : Official Journal of the Society of Magnetic Resonance in Medicine / Society of Magnetic Resonance in Medicine*, *72*(5), 1268–1276. https://doi.org/10.1002/mrm.25041

Uddin, L. Q. (2013). Complex relationships between structural and functional brain connectivity. *Trends in Cognitive Sciences*, *17*(12), 600–602. https://doi.org/10.1016/j.tics.2013.09.011

van den Heuvel, M. P., Mandl, R. C. W., Kahn, R. S., & Hulshoff Pol, H. E. (2009). Functionally linked resting-state networks reflect the underlying structural connectivity architecture of the human brain. *Human Brain Mapping*, *30*(10), 3127–3141. https://doi.org/10.1002/hbm.20737

Vogt, B. A. (2009). *Cingulate Neurobiology and Disease*. Oxford University Press.

Vogt, B. A., Nimchinsky, E. A., Vogt, L. J., & Hof, P. R. (1995). Human cingulate cortex: Surface features, flat maps, and cytoarchitecture. *Journal of Comparative Neurology*, *359*(3), 490–506. https://doi.org/10.1002/cne.903590310

Wang, R., & Reddy, P. H. (2017). Role of glutamate and NMDA receptors in Alzheimer's disease. *Journal of Alzheimer's Disease : JAD*, *57*(4), 1041–1048. https://doi.org/10.3233/JAD-160763

Whitfield-Gabrieli, S., & Nieto-Castanon, A. (2012a). *CONN Toolboox Version 18b*. www.nitrc.org/projects/conn, RRID:SCR_009550

Whitfield-Gabrieli, S., & Nieto-Castanon, A. (2012b). Conn: A Functional Connectivity Toolbox for Correlated and Anticorrelated Brain Networks. *Brain Connectivity*, *2*(3), 125–141. https://doi.org/10.1089/brain.2012.0073

Wong, J. J., O'Daly, O., Mehta, M. A., Young, A. H., & Stone, J. M. (2016). Ketamine modulates subgenual cingulate connectivity with the memory-related neural circuit—A mechanism of relevance to resistant depression? *PeerJ*, *4*, e1710. https://doi.org/10.7717/peerj.1710

Yahya, A., Mädler, B., & Fallone, B. G. (2008). Exploiting the chemical shift displacement effect in the detection of glutamate and glutamine (Glx) with PRESS. *Journal of Magnetic Resonance*, *191*(1), 120–127. https://doi.org/10.1016/j.jmr.2007.12.007

7. Appendices

Network.ROI Name	X Coordinate	Y Coordinate	Z coordinate
DefaultMode.MPFC	1	55	-3
DefaultMode.LP (L)	-39	-77	33
DefaultMode.LP (R)	47	-67	29
DefaultMode.PCC	1	-61	38
SensoriMotor.Lateral (L)	-55	-12	29
SensoriMotor.Lateral (R)	56	-10	29
SensoriMotor.Superior	0	-31	67
Visual.Medial	2	-79	12
Visual.Occipital	0	-93	-4
Visual.Lateral (L)	-37	-79	10
Visual.Lateral (R)	38	-72	13
Salience.ACC	0	22	35
Salience.AInsula (L)	-44	13	1
Salience.AInsula (R)	47	14	0
Salience.RPFC (L)	-32	45	27
Salience.RPFC (R)	32	46	27
Salience.SMG (L)	-60	-39	31
Salience.SMG (R)	62	-35	32
DorsalAttention.FEF (L)	-27	-9	64
DorsalAttention.FEF (R)	30	-6	64
DorsalAttention.IPS (L)	-39	-43	52
DorsalAttention.IPS (R)	39	-42	54
FrontoParietal.LPFC (L)	-43	33	28
FrontoParietal.PPC (L)	-46	-58	49
FrontoParietal.LPFC (R)	41	38	30
FrontoParietal.PPC (R)	52	-52	45
Language.IFG (L)	-51	26	2
Language.IFG (R)	54	28	1
Language.pSTG (L)	-57	-47	15
Language.pSTG (R)	59	-42	13
Cerebellar.Anterior	0	-63	-30
DefaultMode.PCC	1	-61	-38
Cerebellar.Posterior	0	-79	-32

Appendix 1: ROIs used for Intercingulate dFC anaylsis using LEiDA

Subject #	Absolute [Glx] (mmol)	Absolute [Glu] (mmol)	Absolute [Gln] (mmol)	Voxel Tissue Fraction White Matter	Voxel Tissue Fraction Grey Matter	Voxel Tissue Fraction CSF	Corrected [Glx] per Water Tissue Volume (mmol)
1	9.624	7.532	2.092	0.66	0.1	0.24	7.640
2	12.435	9.64	2.813	0.65	0.08	0.27	10.277
3	12.528	10.211	2.317	0.7	0.08	0.22	9.714
4	11.353	9.18	2.173	0.71	0.06	0.23	8.927
5	11.083	8.261	2.823	0.72	0.08	0.2	8.387
6	11.316	8.423	2.894	0.62	0.06	0.32	10.030
7	12.366	9.142	3.224	0.73	0.06	0.21	9.486
8	11.147	9.12	2.027	0.69	0.05	0.26	9.113
9	12.89	9.578	3.312	0.63	0.07	0.3	11.101
10	10.08	7.733	2.347	0.65	0.11	0.24	7.996
11	12.063	10.278	1.785	0.65	0.06	0.29	10.255
12	9.842	7.479	2.363	0.51	0.06	0.43	10.349
13	10.716	8.931	1.785	0.74	0.05	0.21	8.227
14	13.955	9.609	4.346	0.67	0.05	0.29	11.994
15	10.52	9.022	1.498	0.68	0.05	0.27	8.714
16	11.322	8.67	2.652	0.61	0.11	0.28	9.461
17	10.434	8.527	1.907	0.65	0.09	0.26	8.504
18	11.168	8.072	3.096	0.51	0.07	0.41	11.231
19	9.574	8.282	1.292	0.6	0.11	0.29	8.109
20	11.056	9.838	1.219	0.63	0.1	0.27	9.123
21	10.051	7.284	2.767	0.63	0.09	0.28	8.411
22	10.744	8.755	1.989	0.69	0.08	0.23	8.435
23	12.11	9.367	2.743	0.68	0.1	0.23	9.590
24	8.203	7.373	0.83	0.62	0.03	0.35	7.612
25	11.798	9.063	2.753	0.68	0.07	0.26	9.729
26	10.79	9.212	1.578	0.66	0.06	0.28	9.050
27	10.189	9.186	1.002	0.64	0.13	0.24	8.152
28	10.513	8.485	2.028	0.71	0.05	0.24	8.377
29	10.337	8.533	1.784	0.64	0.05	0.31	9.041
30	8.909	6.998	1.912	0.588	0.07	0.35	8.309

Appendix 2: Raw concentration data and voxel tissue fraction.

Brain States	Seeds With Coordinated Activity												
1	i1+	i7-	i8+	s1+	s1-	s2+	s2-	s4-	s5-	s6+	s6-	s7+	
2	i3+	ii3-	i4+	i6-	i7+	i7-	i8+	i8-	i9+	i9-	s2+	s2-	
3	i1-	i2+	i2-	i3+	i3-	i4+	i4-	i7+	i8-	i9+	i9-	s7-	
4	s3+	s3-	s4+	s4-	s5+	s6+	s7-						
5	i1+	i1	i2+	2-	i7+	i7-	i8+	i8-	i9+	s4-	s6-	s7+	s7-
6	i3+	i3-	i4+	i5-	s1+	s1-	s2+	s2-					
7	i3-	i4+	i4-	i5+	i5-	i6+	i6-	s5+					
8	i1+	i1-	i2+	i2+	i2-	s3+	s3-	s4+	s4-	s7+	s7-		

Appendix 3: Intracingulate seeds that have coordinated activity with one another in each ACC brain state.